HHS Public Access
Author manuscript
Matrix Biol. Author manuscript; available in PMC 2022 March 15.

Published in final edited form as:
Matrix Biol. 2020 December ; 94: 31–56. doi:10.1016/j.matbio.2020.07.002.

Periostin and matrix stiffness combine to regulate myofibroblast differentiation and fibronectin synthesis during palatal healing

Georgia Nikoloudaki[a], **Paige Snider**[b], **Olga Simmons**[b], **Simon. J. Conway**[b], **Douglas W. Hamilton**[a,c]

[a] -Department of Anatomy and Cell Biology, and Division of Oral Biology, Schulich School of Medicine and Dentistry, The University of Western Ontario, London, Ontario N6A 5C1, Canada

[b] -Herman B. Wells Center for Pediatric Research, Indiana University School of Medicine, 1044 West Walnut, Indianapolis, IN, United States

[c] -Division of Oral Biology, Schulich School of Medicine and Dentistry, The University of Western Ontario, London, Ontario N6A 5C1, Canada

Abstract

Although the matricellular protein periostin is prominently upregulated in skin and gingival healing, it plays contrasting roles in myofibroblast differentiation and matrix synthesis respectively. Palatal healing is associated with scarring that can alter or restrict maxilla growth, but the expression pattern and contribution of periostin in palatal healing is unknown. Using periostin-knockout (*Postn*$^{-/-}$) and wild-type (WT) mice, the contribution of periostin to palatal healing was investigated through 1.5 mm full-thickness excisional wounds in the hard palate. In WT mice, periostin was upregulated 6 days post-wounding, with mRNA levels peaking at day 12. Genetic deletion of periostin significantly reduced wound closure rates compared to WT mice. Absence of periostin reduced mRNA levels of pivotal genes in wound repair, including α-SMA/*acta2*, *fibronectin* and *βigh3*. Recruitment of fibroblasts and inflammatory cells, as visualized by immunofluorescent staining for fibroblast specific factor-1, vimentin, and macrophages markers Arginase-1 and iNOS was also impaired in *Postn*$^{-/-}$, but not WT mice. Palatal fibroblasts isolated from the hard palate of mice were cultured on collagen gels and prefabricated silicon substrates with varying stiffness. *Postn*$^{-/-}$ fibroblasts showed a significantly reduced ability to contract a collagen gel, which was rescued by the exogenous addition of recombinant periostin. As the stiffness increased, *Postn*$^{-/-}$ fibroblasts increasingly differentiated into myofibroblasts, but not to the same degree as the WT. Pharmacological inhibition of Rac

Corresponding author at: Division of Oral Biology, Schulich School of Medicine and Dentistry, The University of Western Ontario, London, Ontario N6A 5C1, Canada. dhamil2@uwo.ca.

Author contributions

Georgia Nikoloudaki: Methodology, Data curation, Formal analysis, Writing- Original draft preparation.
Paige. Snider: Methodology- Postn mouse generation
Olga. Simmons: Methodology- in situ hybridization Simon. J. Conway: Methodology, Writing - review & editing
Douglas W. Hamilton: Conceptualization, Funding acquisition, Investigation, Supervision, Writing- Reviewing and Editing.

Declaration of Competing Interest

The authors declare no conflict of interest. The funders had no role in the design of the study; in the collection, analyses, or interpretation of data; in the writing of the manuscript, or in the decision to publish the results.

Supplementary materials

Supplementary material associated with this article can be found in the online version at doi:10.1016/j.matbio.2020.07.002.

rescued the deficient myofibroblastic phenotype of *Postn*$^{-/-}$ cells. Low stiffness substrates (0.2 kPa) resulted in upregulation of fibronectin in WT cells, an effect which was significantly reduced in *Postn*$^{-/-}$ cells. Quantification of immunostaining for vinculin and integrin*b*1 adhesions revealed that Periostin is required for the formation of focal and fibrillar adhesions in mPFBs. Our results suggest that periostin modulates myofibroblast differentiation and contraction via integrinβ1/RhoA pathway, and fibronectin synthesis in an ECM stiffness dependent manner in palatal healing.

Keywords

Periostin; Palatal healing; Myofibroblast; Fibronectin; Matrix compliance; RhoA; β1-integrin; Adhesion

Introduction

Wound healing in soft connective tissues, such as skin, is defined as a coordinated series of overlapping events leading to resolution of the defect. Through the phases of hemostasis, inflammation, proliferation and remodeling, concomitant with re-epithelialization, barrier function is re-established [1]. Much of the research related to acute healing has utilized excisional skin wounding, primarily due to ease of defect creation and the use of genetically modified mouse lines [2]. However, different healing profiles have been described. In particular, wound healing in the oral mucosa are known to exhibit significant differences compared with cutaneous injuries [3–5]. In contrast to skin, injuries to the oral mucosa, including gingival tissue, heal rapidly with minimal scar formation [3,4,6,7]. Interestingly, both skin and oral mucosa are characterized by the presence of keratinized epithelium and underlying collagen dense connective tissue. However, while still part of the oral environment, the palatal mucosa is associated with excessive scarring in response to injury [8–10]. Unlike skin and gingiva however, palatal soft tissue is a rigid mucoperiosteum; mucosa and the periosteum are merged and tightly attached to the palatal bone [11].

In recent years, the role of matricellular proteins in each of these phases of healing has become established [12,13]. As a class of proteins, matricellular proteins (MPs) specifically modulate cell-matrix interactions and cell function (adhesion, spreading, migration, proliferation and differentiation) [14] by interacting with cell-surface receptors including integrins. While fibrin, collagen and fibronectin provide structural support to the matrix, defined roles for MPs in the adhesion, migration, proliferation and differentiation of macrophages, fibroblasts, and keratinocytes have been identified post-wounding [12].

Periostin is a secreted matricellular protein associated with wound healing in several connective tissues, with the cell and molecular roles of periostin mainly investigated in collagen-rich biomechanically active tissues [15]. Although knockout mice are viable, periostin deletion results in disruption of several collagenous-based tissues, particularly those subject to constant mechanical loading [16]; severe periodontal disease, significant reduction in bone density, and structural defects in the incisors. Although periostin was defined as a non-structural ECM component, it has been shown to modulate cross-linking and stabilization of the extracellular matrix, including collagen fibrillogenesis [17,18].

Additionally, periostin acts as a scaffold for assembly of several extracellular matrix proteins (type I collagen, fibronectin, tenascin-C, and laminin $\gamma 2$) and accessory proteins (BMP-1 and CCN3) [19–23]. This demonstrates a critical role for periostin in extracellular matrix (ECM) homeostasis and the regulation of cell phenotype.

In skin, we have shown that periostin plays a pivotal role in excisional wound repair, where it facilitates myofibroblast differentiation through a β1 integrin/FAK dependent mechanism [12,24–26]. In contrast, in gingival healing periostin regulates extracellular matrix synthesis, upregulating fibronectin and collagen synthesis via integrin β1, FAK and JNK, but it is not associated with myofibroblast differentiation [27]. The low number of myofibroblasts evident during gingival healing is postulated as an underlying reason for the reduced scar formation evident in healing of the gingival tissue [27]. These contrasting effects on dermal and gingival fibroblasts demonstrate the tissue-specificity of matricellular protein bioactivity in relatively homologous tissues [28]. The palatal mucoperiosteum, even though part of the oral cavity, has been shown to exhibit significant scarring after surgical procedures. The investigation of distinct healing patterns among skin, gingiva and the palatal mucoperiosteum could provide deeper understanding of how differences in molecular composition and physical properties of these tissues lead to the different healing outcomes. It would therefore be intriguing to assess the role of periostin in palatal tissues, which while still in the oral cavity, is strongly associated with scarring after injury. However, the role of periostin in palatal mucoperiosteum has yet to be investigated.

It remains critical to fully understand the underlying molecular and cellular mechanisms responsible for ECM accumulation in the palate during the wound healing process. Verstappen et al., using a rat model, found that there are significantly more myofibroblasts in the wounded mucoperiosteum than are evident in skin wounds, which they attributed to the different contractile abilities that these tissues possess and correlated their findings with the different wound healing patterns of these tissues [29]. We hypothesized that periostin would be transiently upregulated following palatal wounding, modulating fibroblast differentiation and matrix synthesis. Using a periostin-knockout (*Postn*$^{-/-}$) mouse [16], we show that the loss of periostin results in altered wound closure kinetics. In contrast to gingiva, α-SMA myofibroblasts are present during palatal healing, and genetic deletion of periostin resulted in reduction of α-SMA and fibronectin in the newly formed granulation tissue. Furthermore, murine palatal fibroblasts isolated from *Postn*$^{-/-}$ mice showed an impaired contraction of a collagen matrix, which can be rescued by the exogenous addition of periostin. Furthermore, using silicon substrates of different elastic modulus, we show that *Acta2*/α-SMA is upregulated in stiff substrates and fibronectin is upregulated in low stiffness conditions, and that these effects were attenuated by the genetic deletion of periostin, suggesting *that the ECM stiffness is an important modulator of cell behavior*.

Results

Periostin mRNA and protein are up-regulated after excisional palatal wounding and peak 12 days after wounding

To temporally investigate the palatal healing process, we quantified the closure of the palatal mucoperiosteum in C57Bl/6 WT mice at 3, 6, 9, 12 and 15 days post-wounding, with

unwounded palatal mucoperiosteum serving as a structural baseline control (day 0) (Fig. 1). Analysis of in vivo *Postn* gene expression during palatal wound healing in wild-type (WT) mice by real-time quantitative polymerase chain reaction (RT-qPCR) showed that *Postn* mRNA levels were significantly increased during palatal wound repair at day 6 ($P < 0.05$), peaking at day 12 ($P < 0.01$) (Fig. 1A). Using *in situ* hybridization (ISH) (Fig. 1B) and immunofluorescent staining (Fig. 1C), in normal unwounded palatal mucosa periostin signal was weakly detected in the basal lamina and periosteum covering the palatal bone, with intense signal at the periodontal ligament of neighbouring teeth (arrow-Fig. 1B, white arrowheads Fig. 1C). After wounding, periostin was detected throughout the ECM of the granulation tissue at days 6, 9, 12 and 15 (Fig. 1B, C).

Genetic deletion of periostin results in altered wound-closure kinetics during excisional palatal healing in mice

To investigate the contribution of periostin to palatal wound repair process, full-thickness excisional wounds were created in *Postn*$^{-/-}$ (KO) and *Postn*$^{+/+}$ (WT) mice. To assess differences in the rate of wound closure between *Postn*$^{-/-}$ and WT mice, we measured wound size based on gross appearance up to 12 days after wounding. Genetic deletion of *Postn* significantly reduced wound closure rates compared to WT mice. Wounds in WT mice were macroscopically resolved by day 6, with wound size in *Postn*$^{-/-}$ animals reduced by 80% of the initial wound area (Fig. 2A, B). Histological analysis of sections from the center of the wounds at day 6 (C-F) confirmed that *Postn*$^{-/-}$ wounds were significantly larger than those of their WT littermates ($P < 0.05$) with decreased re-epithelialization at day 6 evident in *Postn*$^{-/-}$ mice ($P < 0.01$), although epithelial tongue length was similar in both genotypes ($P > 0.05$). Wounds in both WT and *Postn*$^{-/}$ were closed by day 12.

Absence of Postn alters transcriptional regulation of genes associated with repair and wound healing

α-SMA expression is attenuated in the granulation tissue of *Postn*$^{-/-}$ mice—*Acta2* is expressed by mesenchymal cell types including pericytes and myofibroblasts (MF). MFs are key during wound healing, responsible for ECM synthesis, remodeling and tissue contraction [30–32]. Assessment of α-SMA in *Postn*$^{-/-}$ and WT wounds using immunohistochemistry showed α-SMA was evident at the wound edge and within the granulation tissue of WT wounds at days 6 and 9. At day 6, increased immunoreactivity of α-SMA was detected at the wound border in WT mice, throughout the granulation tissue and in blood vessel walls (Fig. 3A). In day 6 *Postn*$^{-/-}$ wounds, α-SMA immunoreactivity was reduced when compared with that in WT. Quantitative PCR (RT-qPCR) on RNA isolated from WT and *Postn*$^{-/-}$ wounds at 3, 6, 9, 12, and 15 days post wounding demonstrated that *Acta2* mRNA levels were increased in both genotypes, but the copy number was significantly reduced in the granulation tissue of *Postn*$^{-/-}$ mice at day 6 (Fig. 3B) ($P<0.05$). Double immunofluorescence staining was used to detect the spatial relationship between α-SMA and periostin signal in the wound matrix. We observed that α-SMA positive cells, indicating the presence of myofibroblasts, were in lying within the granulation tissue and periostin matrix, indicating that periostin might have an effect to myofibroblast differentiation by direct contact (Fig. 3D). To determine whether the reduction in SMA mRNA levels was due to impaired fibroblast recruitment into the granulation tissue,

sections were labeled for fibroblast-specific protein-1 (FSP-1) (Fig. 4A, B) and vimentin (Fig. 4C). While no significant differences in FSP-1 immunoreactivity in *Postn*$^{-/-}$ tissue compared to WT at days 6 and 9 post-wounding, we observed decreased vimentin signal in *Postn*$^{-/-}$ wounds at day 6 when compared to WT wounds indicating impaired granulation tissue formation and reflecting the delay in wound healing kinetics (Fig. 4D).

Genetic deletion of Postn is associated with reduced fibronectin expression and deposition during palatal healing—Using immunofluorescence, we next assessed localization of fibronectin, a glycoprotein important in ECM organization and stability, as well as attachment sites for fibroblasts and keratinocytes, to facilitate their migration into the wound bed [33,34]. Fibronectin immunoreactivity was evident in the basal lamina and at the granulation tissue of WT wounds at day 6 and 9. However, in *Postn*$^{-/-}$ wounds the granulation tissue at the wound edge had reduced fibronectin labeling (Fig. 5A). Analysis of *in vivo Fn1* mRNA levels by RT-qPCR confirmed that copy number of *Fn1* was significantly lower in *Postn*$^{-/-}$ wounds compared to WT at day 9 post-pounding ($P < 0.001$) (Fig. 5C). Using double immunofluorescence staining we found that fibrillar fibronectin and periostin partially colocalize within the wound environment, further supporting the direct interaction if these biomolecules (Fig. 5B)

Genetic deletion of Postn affects immune cell infiltration—Inflammatory cell infiltration in the wounds was assessed by characterizing the macrophages populations in the granulation tissue of the wounds using antibodies specific for iNOS (M1 polarization), and arginase-1 (arg-1) (M2 polarization) [35]. Overall, WT wounds appeared to have increased M1 and M2 macrophages than *Postn*$^{-/-}$ during wound healing at day 3, 6 and 9 post wounding. The presence of iNOS-positive cells was more abundant in day 6 and 9 WT wounds throughout the granulation tissue (Fig. 6), as well as immunoreactivity in the epithelial layers. However, *Postn*$^{-/-}$ wounds had significantly less iNOS-positive cells (WT, 30%; Postn$^{-/-}$,12%; $P < 0.001$), which were located at the edge of the wound (Figure A, C). Similar observations were also found for Arginase-1-positive cells. These observations suggest that the reduced number of macrophages in palatal healing likely results from genetic deletion of periostin.

βigh3 does not have a compensatory role for the loss of periostin in Postn$^{-/-}$ animals—Also defined as a matricellular protein, transforming growth factor-β-induced gene product-h3 (TGFBI/βigh3)is considered a paralog of Postn because of their structural similarity [36]. *In vitro* studies showed that βigh3 promotes adhesion and migration of dermal fibroblasts and keratinocytes [37–39]. Thus, we hypothesised that βigh3 might play compensatory roles in the adhesion and migration of keratinocytes/fibroblasts at wound sites. We therefore assessed the levels of *TGFBI/βigh3* by ISH and RT-qPCR in WT and *Postn*$^{-/-}$ embryonic tissues as well as its expression in normal and wounded tissues. ISH demonstrated that *βigh3* mRNA is present in normal, uninjured palate and is upregulated during wound healing. *β*igh3 showed increased expression in comparison to Postn in day 3 wounds, where it is present in granulation tissue filling the wound site (Supplemental data-Fig. 1A). At day 6 post-wounding both *Postn* and *βigh3* are present in WT granulation tissue at the wound site, after which they are gradually reduced. RT-qPCR analysis confirmed that

the mRNA level of *βigh3* in day 6 *Postn*$^{-/-}$ wounds is significantly reduced compared to WT wounds ($P < 0.05$). The different wound-response spatiotemporal expression patterns of these two matricellular proteins might be an indication that βigh3 may not compensate for the loss of Postn during palatal wound healing or that *Postn* and *βigh3* are differentially regulated via divergent upstream signaling pathways. This is supported by our observations in embryonic tissues where *Postn* mRNA message is present in the developing palatal shelves of the secondary palate and tongue at E15, while *βigh3* mRNA message is only present in the tongue (Supplemental data-Fig. 1C). Thus, βigh3 can play an independent role and exhibit non-overlapping expression and function with Postn in the development of the hard palate in mice.

Canonical TGFβ signaling is not altered in Postn−/− fibroblasts

TGFβ is known to cause an increase in α-SMA expression through phosphorylation of Smad3 [40], and plays a major role in myofibroblast differentiation [41]. Therefore, to determine whether the reduction in α-SMA expression and immunoreactivity in *Postn*$^{-/-}$ granulation tissue was due to defective TGFβ Smad3 signaling, we assessed the number of nuclei positive for phosphorylated Smad2 and Smad3 (pSmad2/3) within the granulation tissue of palatal wounds at day 3, 6, 9, 12 and 15 post-wounding (Fig. 7A). The number of pSmad2/ 3-positive nuclei was similar in both WT and *Postn*$^{-/-}$ wounds, suggesting that canonical TGFβ signaling is active in *Postn*$^{-/-}$ wounds and unaffected by the absence of periostin (Fig. 7B).

Exogenous periostin is sufficient to induce a contractile phenotype in *Postn*$^{-/-}$ fibroblasts

To examine the functional role of periostin in palatal healing, we utilized *in vitro* assays to investigate how genetic deletion of periostin affects the proliferation rate and myofibroblast differentiation of murine palatal fibroblasts (mPFBs). Periostin is known to modulate expression of α-SMA during skin healing [25], but not in gingival healing [27]. In our in vivo experiments we observed a reduced levels of α-SMA on *Postn*$^{-/-}$ wounds (2.3.1) which indicates that a defect might exist in differentiation of fibroblasts to myofibroblasts in *Postn*$^{-/-}$ wounds. When cells where cultured for 24 and 72 h on tissue culture plastic (TCP), *Acta2* mRNA levels were significantly higher in WT mPFBs in comparison to *Postn*$^{-/-}$ mPFBs ($P < 0.01$, $P < 0.001$) (Fig. 7C). Exogenous stimulation of the cells with TGFβ (5 ng/ml) did not have a significant effect on Acta2 mRNA levels in either cell type (7D), indicating that the cells might have already become maximally differentiated.

WT and *Postn*$^{-/-}$ mPFBs were isolated and cultured for 1,3,5 and 7 days to assess their proliferation rates. Both cell types exhibited a 4-fold increase in cell number by day 7 with no significant difference in cell number evident between the genotypes ($p > 0.05$) (Fig. 7E). To assess the contractile ability of the cells we utilized in vitro assays to determine their ability to contract a floating collagen gel. Quantification of contraction through measurement of gel weight showed that WT palatal fibroblasts were able to significantly contract the collagen matrix in comparison with *Postn*$^{-/-}$ palatal fibroblasts, indicating that periostin is required for contraction of a collagen matrix by palatal fibroblasts ($P < 0.01$) (Fig. 7F). To further investigate this finding, 5 mg/ml recombinant human periostin (rhPN)

was added to the collagen matrix and was found to be sufficient to induce contraction of the gels by *Postn*$^{-/-}$ palatal fibroblasts.

ECM stiffness regulates cell behavior

Periostin expression in mPFBs is regulated by matrix stiffness—To evaluate whether Periostin is differentially regulated by the stiffness of the underling substratum, mPFBs were seeded for 24- and 72 h on substrates of different stiffness. Up to 24 h post seeding, *Postn* expression levels were similar across different stiffness substrates (Fig. 8A). At 72 h, Postn mRNA levels were significantly higher in very stiff substrates (TCP) ($P < 0.01$, $P < 0.05$) (Fig. 8B), reducing gradually as the stiffness of the substrate decreases.

Matrix stiffness is not sufficient to restore the contractile phenotype of *Postn*$^{-/-}$ cells—Differentiation of fibroblasts into myofibroblasts requires TGFβ-dependent signaling, but also depends heavily on increased matrix stiffness [31,42,43]. To explore the contribution of microenvironment stiffness on cellular behavior, WT and *Postn*$^{-/-}$ mPFBS were seeded on silicone substrates with different Young's elastic modulus simulating different scar maturation stages, and *Acta2*/α-SMA expression was evaluated using RTqPCR, immunolabeling and western blotting. Murine palatal fibroblasts seeded on collagen-coated tissue culture plates (TCP) adopted a planar, well-spread morphology typical of fibroblasts in culture (Fig. 8A). These cells developed very distinct stress fibers, which often incorporated α-SMA, indicating myofibroblast differentiation. Depending on the stiffness of their environment, after 24 h culture cells assume differentiated myofibroblast characteristics on tissue culture plastic (TCP-control) and "fibrosis-rigid" (65 kPa) substrate, formed α-SMA-negative stress fibers on "normal tissue soft" (8 kPa) substrates, while on very soft "granulation tissue soft" (0.2 kPa) substrates the cells were characterized by poor spreading and exhibited no contractile bundles (Fig. 8A).

The percentage of fibroblasts with positive- α-SMA stress fibers increased with an increase in substrate stiffness ($P < 0.001$). The proportion of WT mPFBs with α-SMA-positive stress fibers peaked on TCP at 76%, while on substrates of low stiffness (0.2 kPa) that proportion accounted only for the 26% of the cells (Fig. 8C, D). Compared with WT mPFBs, the proportion of *Postn*$^{-/-}$ cells with α-SMA-positive stress fibers was significantly lower on TCP (54%) ($P<0.01$) and 0.2 kPa (9%) ($P<0.05$) substrates. These observations were further supported by *Acta2* expression levels and α-SMA protein levels (Fig. 8F, G), showing that the absence of periostin in *Postn*$^{-/-}$ cells resulted in reduction of acta2/α-SMA expression which was mainly manifested in very stiff conditions (TCP). When cells were treated with 5 ng/ml TGFβ, the proportion of *Postn*$^{-/-}$ cells with α-SMA-positive stress was similar to WT cells on 0.2 kPa substrates (WT, 20%; *Postn*$^{-/-}$, 23%) (Fig. 8E).

Fibronectin secretion is regulated by periostin and matrix stiffness—To mimic the in vivo conditions and validate our observations regarding the deficit in fibronectin deposition in *Postn*$^{-/-}$ wounds, WT and *Postn*$^{-/-}$ mPFBs were seeded on silicone substrates with different Young's elastic modulus. Low stiffness substrates (0.2 kPa) resulted in upregulation of fibronectin in WT cells, when compared to control (TCP) ($p<0.05$). Similar to our in vivo observations, genetic deletion of periostin in *Postn*$^{-/-}$ mPFBs resulted in a

trend of reduced fibronectin mRNA levels across all different substrates, a difference which was significant at low stiffness substrates (0.2 kPa) ($P<0.05$), indicating two important regulators of fibronectin synthesis during palatal healing: periostin and microenvironment stiffness (Fig. 9).

Periostin modulates myofibroblast differentiation in palatal fibroblasts via RhoA/ROCK pathway—Periostin has been shown to increase focal adhesion formation, α-SMA levels and collagen contraction in fibroblasts from hypertrophic scars, effects which were dependent on Rho-associated protein kinase [26]. To identify the signaling pathway intermediates that are activated by periostin and/or matrix stiffness and control myofibroblast differentiation and fibronectin synthesis, we utilized pharmacological inhibitors for RhoA, Y-27632, and Rac1, Z62954982. We found that both WT and *Postn*$^{-/-}$ cells on an extremely stiff environment (TCP) exhibit well spread morphology with formation of stress fibers, although in *Postn*$^{-/-}$ cells the incorporation of α-SMA in the stress fibers is reduced (53%) when compared to the WT (72%) ($P<0.01$). Rho inhibition (Y-27632) resulted in cytoskeleton remodeling characterized by a dendritic phenotype with large cytoplasmic protrusions, and complete loss of α-SMA in both cell genotypes (WT, 17%; *Postn*$^{-/-}$, 14%). Interestingly, the inhibition of RhoA on 0.2 kPa conditions did not have as prominent effect on the cytoskeletal configuration as is evident on TCP, suggesting that Rho is not active in highly elastic environments (Fig. 10A). When the pharmacological inhibitor for Rac1 was used to drive ROCK activation, the development of α-SMA-positive fibers was restored in both WT (78%) and *Postn*$^{-/-}$ (70%) ($P>0.05$) cells seeded on TCP, suggesting that periostin modulates myofibroblast differentiation in stiff matrices via RhoA pathway (Fig. 10A, B). On 0.2 kPa substrates, the addition of the pharmacological inhibitor to Rac1 was not sufficient to stimulate the formation of α-SMA stress fibers and myofibroblast differentiation in either cell type (WT, 2%; *Postn*$^{-/-}$,1.8%) (Fig. 10A, C).

We next investigated the effect of RhoA or Rac inhibition on fibronectin synthesis. RhoA inhibition resulted in reduced fibronectin matrix assembly in both WT and *Postn*$^{-/-}$ cell types (Suppl. figure 2). In contrast, direct activation of RhoA through Rac inhibition restored fibronectin matrix assembly and protein levels similar to control levels (DMSO) in both WT and *Postn*$^{-/-}$ mPFBs, supporting that fibronectin matrix synthesis and assembly requires Rho kinases (ROCK). However, these results suggest that the mechanism through which Periostin regulates fibronectin synthesis in mPFBs does not depend on RhoA/ROCK pathway.

Periostin is required for the formation of focal and fibrillar adhesions in mPFBs—Organization of adhesion sites is controlled not only by the integrin-ligand interactions, but also the physical properties of the extracellular matrix which modulate local tension at the adhesion sites [44]. To investigate how a change in the stiffness of the cell microenvironment (using culture substrates) affects the assembly of different types of adhesion complexes in the presence or absence of periostin, WT vs *Postn*$^{-/-}$ cells were seeded on substrates of different elastic modulus. To determine whether the absence of periostin in *Postn*$^{-/-}$ mPFBs result in defective adhesion complexes formation, we visualized focal (vinculin) and fibrillar adhesions (integrin-β1) using immunocytochemistry,

and we quantified the number of adhesions/cell, the total adhesion area/cell and the average adhesion area/cell adhesion using ImageJ. The number and the size of focal adhesions as well as the total focal adhesion area increased with an increase in substrate stiffness (Figs. 11, 12A–C). In the absence of periostin the number of focal adhesions per cell, the size of the focal adhesions and the focal adhesion area per cell were significantly reduced across all different substrates. More specifically, on very stiff substrates (TCP) *Postn*$^{-/-}$ cells had significantly less focal adhesion sites/cell (n = 383±99) when compared to WT cells (n = 672±111) (P<0.05), and their average size was smaller (WT, 5 ± 1μm^2; *Postn*$^{-/-}$, 4 ± 0.7μm^2) resulting in a significantly smaller total adhesion area per cell in *Postn*$^{-/-}$ cells (WT, 3238±686μm^2; *Postn*$^{-/-}$, 1535±645μm^2) (P<0.05). On low stiffness substrates (0.2 kPa) the average size of the focal adhesions (1.9 ± 0.1μm^2) and the number of adhesion sites per cell (n = 117±63) were significantly smaller when compared to WT cells (3.2 ± 0.4μm^2; (P<0.01), n = 267±81; P<0.05). Investigating the effect of the genetic deletion of Periostin in fibrillary adhesion formation, we found that the percentage of β1-integrin-positive adhesion area/cell (Fig. 12E) and the levels of β1-integrin expression (Fig. 12F) were significantly reduced in *Postn*$^{-/-}$ cells when compared to WT cells. These effects were more prominent when the cells were cultured on substrates of low stiffness and could provide a potential explanation of reduced fibronectin synthesis by *Postn*$^{-/-}$ mPFBs under these conditions.

Discussion

Periostin, a secreted ECM protein, is transiently expressed during normal cutaneous [25] and gingival wound repair [27], but is overexpressed and persistent in abnormal scars and other benign fibroses that are characterized by fibroblast proliferation and myofibroblast differentiation [19,24,26]. Excessive scarring as a consequence of cleft palate reconstruction surgery results in restriction of the normal maxillary development in transversal width when the patient is in their growing phase, leading to serious functional and esthetic problems [45]. The expression profile and potential roles of periostin in palatal healing have never been investigated. On the contrary, wounds in gingival tissues and the oral mucosa heal faster, with minimal scar formation in comparison to skin wounds [3,4,6,7], which is concomitant with reduced inflammatory response, attributed to the reduced recruitment of neutrophils, macrophages, and T-cell [6,7]. Several other contributory factors have been proposed to be involved, such as the presence of saliva, leukocytes, growth factors, phenotypic differences between oral and cutaneous fibroblasts [6,46], and the absence of myofibroblasts [27]. The distinct healing patterns among skin, gingiva and the palatal mucoperiosteum, and the contrasting tissue-specific effects of periostin's bioactivity [28], could provide deeper understanding of how differences in molecular composition and physical properties of these tissues lead to the different healing outcomes. Applying this translatable knowledge in the fields of biotechnology, these specific biomechanical cues can be targeted and guided to enhance healing outcomes while inhibiting undesired effects, such as scarring ang fibrosis [47]

In this study, we show that the loss of Postn by use of the *Postn*$^{-/-}$ mouse [16] results in altered palatal wound-closure kinetics, especially during the proliferation phase of wound healing. The alteration in wound closure corresponds with the onset at day 6, but not the peak of Postn expression at day 12 post-wounding in WT animals. Wounds in WT mice

were considered closed by day 6, but wounds in *Postn*$^{-/-}$ were completely closed at day 12 post-wounding (Fig. 2A, B, Fig. 3). Although the histological analysis of sections from the center of the wounds at day 6 showed decreased re-epithelialization in *Postn*$^{-/-}$ mice, the epithelial tongue length (epithelial migration distance) was similar in both genotypes. The latter is considered a more reliable method for measurement of wounds of different [25,48]. Periostin has been shown to regulate myofibroblast differentiation, matrix synthesis and re-epithelialization in skin [17,24,25]. Previous studies, including by our group, have shown that following excisional skin wounding in mice, periostin is upregulated at day 3, levels peak at day 7, after which expression eventually returns to baseline [49]. In gingival wound healing, using gingivectomy defects in rats [27], periostin expression was increased at day 7, with protein levels increased yet further at day 14 in the ECM of the connective tissue. While assessment of gingival healing in the *Postn*$^{-/-}$ mice would be the most direct method, it is technically challenging due to the size of the gingiva and that any defect created in the gingival tissue heals rapidly limiting timepoints for analysis. In a similar manner to skin and gingival healing, periostin upregulation in palatal mucoperiosteum coincides with the proliferative and remodeling phases of healing, but not the inflammatory phase. Interestingly, periostin protein levels are not increased at day 3 as is seen in skin healing [50], highlighting a difference in expression profile between the two tissue types.

We have previously shown that during skin healing myofibroblast differentiation mediates contraction of the wound edges and is modulated by periostin in mice [25], but during gingival healing we observed a very low level of myofibroblasts, suggesting that adoption of a contractile myofibroblast phenotype is not a significant event in gingival wound healing [27], providing a potential explanation of the scarless healing of the latter. After formation of actin-myosin contractile bundles, stress fibers, it is the neoexpression and incorporation of α-SMA that significantly augments the contractile activity of activated myofibroblasts [51]. In the current study, immunohistochemistry and RT-qPCR reveal that α-SMA/*Acta2* is up-regulated in the palatal wounds during wound healing, but it was significantly reduced in the granulation tissue of *Postn*$^{-/-}$ mice at day 6 when compared with that in WT controls. These results further support that the palatal mucoperiosteum has different healing potential than the gingival tissue and could provide a potential therapeutic target for palatal scarring.

To determine whether the reduction in α-SMA expression was due to impaired fibroblast recruitment into the granulation tissue, wound sections were labeled for fibroblast-specific protein-1 and vimentin. Cell numbers showed no significant differences in FSP-1 immunoreactivity in *Postn*$^{-/-}$ wounds compared to WT, suggesting that genetic deletion of periostin does not affect fibroblast recruitment, but rather result in deficient contractility. To further investigate this finding, we sought to determine whether reduced α-SMA within *Postn*$^{-/-}$ granulation tissue was the result of a defect in differentiation of fibroblasts into myofibroblasts. Supporting this hypothesis, isolated palatal fibroblasts (mPFBs) from *Postn*$^{-/-}$ animals did not have any differences in their proliferation rate when compare to cells isolated from WT animals and showed significant reduction in their ability to contract a collagen gel. Addition of exogenous rhPN, however, fully rescued the phenotype of the *Postn*$^{-/-}$ fibroblasts suggesting that periostin is required for gel contraction and its presence in the extracellular matrix is sufficient to induce a contractile myofibroblast phenotype. While similar observations have been reported in murine dermal fibroblasts isolated from

Postn$^{-/-}$ animals, highlighting the role of periostin in skin healing as a modulator of myofibroblast differentiation and contraction [25], in gingival fibroblasts the exogenous addition of rhPN does not increase α-SMA protein nor induce gel contraction [27], further supporting the behavioral and phenotypic differences between gingival, palatal and dermal fibroblasts observed in vitro. Interestingly, in spite of the relative similarity of fibroblasts in connective tissues, not only is there strong evidence about the existence of different phenotypes, but also it has been proven that these phenotypes are substantially variable among different anatomical regions [52,53]. These phenotypic differences have been proposed to be partially responsible for the different healing patterns of the tissues [46,54]. Recently, Mah et al. 2014 tried to shed light on the relation between the distinct phenotypes of gingival fibroblasts and skin fibroblasts and their different wound healing patterns in 3D cell cultures. They found that gingival fibroblasts proliferate faster and express higher levels of molecules involved in modulation of inflammation and ECM remodeling (MMP-1, −3, −10, TIMP-4), while skin fibroblasts displayed significantly higher expression of fibrillar (collagens and elastin) and non-fibrillar (SLRPs and matricellular proteins) ECM proteins, and molecules involved in TGF-β signaling, regulation of myofibroblast phenotype and cell contractility, such as TGF-β1,-β2, -β3, Smad, α-SMA, CXCL12, Cadherin-2, −11. Their findings are indicative that gingival fibroblasts display a phenotype that may promote faster resolution of inflammation and ECM remodeling, which is characteristic to reduced scar formation, while skin fibroblasts have a profibrotic, scar-prone phenotype [55]. On the contrary, our results provide evidence for the fibroblast heterogeneity among oral mucosa tissues, the absence of myofibroblast differentiation during both healing and scarring of the gingiva [27,56] suggest significant epigenetic differences compared to palatal fibroblasts.

Mechanical tension [51,57,58] and TGFβ secretion and activation during wound healing and ECM remodeling [41,59] determine the percentage of differentiated, α-SMA-positive myofibroblasts [31,41,43]. For the induction of α-SMA by *TGF*β, phosphorylation of FAK is required, which is a central molecule activated in adhesive signaling [60]. We have previous shown that in murine skin, periostin modulates α-SMA expression in a FAK and integrin-β1 engagement dependent manner [25]. To determine whether the reduction in α-SMA expression and immunoreactivity in *Postn*$^{-/-}$ granulation tissue was due to defective TGFβ Smad3 signaling, we assessed the number of nuclei positive for phosphorylated Smad2 and Smad3 (pSmad2/3) within the granulation tissue of palatal wounds. No differences were observed in the number of pSmad2/ 3-positive nuclei between WT and *Postn*$^{-/-}$ wounds, suggesting that canonical TGFβ signaling is active in *Postn*$^{-/-}$ wounds. In mPFBs, pharmacological inhibition of FAK pathway did not have any effect on α-SMA/Acta2 expression (Supplemental Data-Fig. 3C, D) suggesting that periostin modulates α-SMA expression through an alternative mechanism. These observations shift our focus to investigate the role of ECM stiffness and adhesive signaling as potential modulators of periostin-induced myofibroblast differentiation.

Mechanical stress exerted by the stiffness of ECM positively feedback on the development and progression of fibrotic conditions by directly promoting myofibroblast activation and persistence through various mechanotransduction pathways [43], [58, 61–63]. Building on our previous studies [25,27], the differences observed in skin, gingival and palatal healing processes suggest that the ECM of these tissues may possess different level of stiffness.

Changing the stiffness of the cell substrate is an efficient method to control myofibroblast activation in vitro [31,57,58]. To explore how periostin and microenvironment stiffness influence cellular behavior, cells isolated from WT and *Postn*$^{-/-}$ palates were seeded on collagen-coated silicon substrates with different Young's elastic modulus. Here we show that myofibroblast differentiation of mPFBs is stimulated by culture on stiff culture substrates (TCP, 64 kPa) but suppressed on substrates mimicking normal tissue (8 kPa) or granulation tissue (0.2 kPa) ECM stiffness, which is in agreement with other reports [62]. Our results are consistent with studies demonstrating that mesenchymal stem cells, different fibroblasts, and hepatic stellate cells all remain relatively inactive on culture substrates mimicking the stiffness of normal tissue [64–66]. *Postn*$^{-/-}$ mPFBs showed lower expression *Acta2*/α-SMA levels suggesting impaired myofibroblast differentiation capacity when compared to WT cells, which was manifested in rigid, collagen-coated tissue culture plates (TCP). We then sought to investigate whether α-SMA is incorporated in stress fibers of the cells using immunocytochemistry and we found significantly lower proportion of *Postn*$^{-/-}$ cells with α-SMA-positive stress fibers on TCP and 0.2 kPa substrates when compared to WT cells, but these differences where not observed in the intermediate stiffness conditions (64 kPa, 8 kPa). These observations indicate that in palatal fibroblasts periostin modulates myofibroblast differentiation in cases of extreme stiffness and in very compliant microenvironments. Our observations from the in vivo experiments in the palate show that α-SMA is still present but reduced in the granulation tissue of *Postn*$^{-/-}$ wounds, indicating that the loss of periostin is partially compensated by the stiffness of ECM environment which is sufficient to drive myofibroblast differentiation in *Postn*$^{-/-}$ wounds. On the contrary, during healing of excisional wound in murine skin, genetic deletion of periostin does not affect α-SMA expression in high-tension areas at the wound edge, while α-SMA is completely absent in the relatively low-tension granulation tissue, suggesting that in skin periostin modulates myofibroblast differentiation in relatively compliant tissue [25]. On the contrary, in gingival healing the presence of periostin is not sufficient to induce α-SMA [27]. Our observations in the palate highlight the distinct characteristics of the palatal soft tissue, which is an environment of increased stiffness, where, as a rigid mucoperiosteum, the mucosa and the periosteum are merged and tightly attached to the underlying palatal bone.

We next examined whether genetic deletion of periostin alters the production of fibronectin, a key ECM component. Fibronectin is a glycoprotein found in plasm and in the ECM of tissues and is expressed by multiple cell types different cells which comes in different splice variants. It is involved in myofibroblast and TGFβ1 activation [34,67, 68], plays a key role in cell adhesive and migratory behavior, is a regulator of collagen organization and tissue phenotype [34,69,70], and is elevated in fibrosis [71]. Extracellularly, periostin directly binds to fibronectin through the EMI domain [17,72]. Intracellularly, it has been observed a proximal localization between periostin and fibronectin in the endoplasmic reticulum of fibroblastic cells indicating that the two proteins interact before fibronectin's secretion [73], and evidence suggests that periostin enhances secretion of fibronectin from the endoplasmic reticulum to the extracellular environment [23,73]. Our in vivo data from RT-qPCR and immunolabeling assays showed that fibronectin is increased during palatal healing, but *Postn*$^{-/-}$ wounds had significantly less fibronectin than WT wounds. This observation further supports our previous finding, where human gingival fibroblasts cultured

in the presence rhPN had increased fibronectin production, an effect which was attenuated by pharmacological inhibition of FAK and JNK signaling [27]. In mPFBs, pharmacological inhibition of FAK pathway did not have any effect on fibronectin expression (Supplemental Data Fig. 3A, B).

To explore whether the microenvironment stiffness influences fibronectin expression, we cultured mPFBs isolated from WT *and Postn*$^{-/-}$ animals on silicon substrates of different stiffness. On very stiff substrates the cells acquired a contractile phenotype with upregulation of α-SMA and down-regulation of fibronectin. Fibronectin synthesis was up-regulated in conditions of low stiffness (0.2 kPa), but genetic deletion of periostin in *Postn*$^{-/-}$ cells resulted in significantly reduced fibronectin expression compared to WT cells. Taken together, our findings provide further evidence of the role of periostin as a modulator of fibronectin synthesis. A potential mechanism of fibronectin synthesis modulation by periostin is via integrin β1. Cells mediate fibronectin matrix assembly through integrin binding to the RGD binding domain [69]. The primary receptor for fibronectin matrix assembly is α5β1. Receptor binding stimulates fibronectin self-association and organizes the actin cytoskeleton to promote cell contractility. Fibronectin conformational changes expose additional binding sites that participate in fibril formation and in conversion of fibrils into a stabilized, insoluble form. Once assembled, the fibronectin matrix impacts tissue organization by contributing to the assembly of other ECM protein [34,69]. Our in vitro results show that β1-integrin expression is significantly reduced *in Postn*$^{-/-}$ cells compared to WT cells when cultured on low stiffness substrates, providing an additional explanation of reduced fibronectin synthesis by *Postn*$^{-/-}$ mPFBs under these conditions.

Cells are subjected to mechanical stresses and receive and respond to stimuli from the ECM through integrins. The coupling of internal and external forces through integrins allows the cells to structurally modify the ECM through cytoskeletal forces that pull on integrins and to respond to external forces by remodeling their cytoskeleton [74,75]. β1 integrins are the primary plasma membrane receptors transmitting tensional forces from the actin cytoskeleton to the extracellular matrix [76,77]. Myosin-II-mediated contractility is required for cells to actively sense changes in the rigidity of the extracellular matrix [78,79]. The action of myosin II along actin stress fibers maintains the basal tension on the cell-matrix adhesions. This basal tension enables mechanosensitive focal adhesion proteins to sense the increase in resistance, which results when the basal actomyosin tension pulls on a more rigid extracellular matrix. The increased tension at focal adhesions can cause calcium influx through stretch-activated calcium channels, trigger the integrin-dependent activation of FAK and Src, and change the conformation of certain mechanosensing proteins, such as p130Cas, talin and vinculin, to initiate intracellular signaling and mechanotransduction [74]. In this study we found that focal adhesion formation and size are increased with an increase in the stiffness of the cell microenvironment, and that the genetic deletion of Periostin resulted in a significant defect in focal adhesion formation in *Postn*$^{-/-}$ cells. This finding provides a possible explanation of the reduced contractility and fibronectin synthesis in the absence of Periostin. Collectively, we found that in the absence of Periostin, the formation of both focal and fibrillar adhesions is defective demonstrating the direct functional role of periostin in adhesion properties of the cells.

Rho signaling also plays key roles in mechano-transduction: The RhoA ROCK myosin-II signaling axis is capable of sensing changes in the structure of the extracellular matrix and responding to it by increasing actomyosin contractility [80]. Activation of RhoA (ROCK) promotes stress fibers maintenance, increases ECM tension, integrin clustering and the formation of large focal adhesion complexes [80]. Further, a recent study shows that β1 and β3 integrins binding and interaction regulate in a reciprocal, antagonizing manner each others' activities in the regulation of intercellular adhesion and collective cell migration by Rho GTPase activities [81]. Also, it has been shown these kinases (ROCK I & II) play a significant role in fibronectin matrix assembly and are implicated in microfilament bundle assembly and smooth muscle contractility [82,83]. An important feature of this mechanical signaling network is the crosstalk between Rac1 and RhoA signaling that potentially regulates the mechanosensing of matrix rigidity, as well as the contribution of extrinsic soluble factors, such as growth factors or cytokines, which can modulate RhoA activity to increase or decrease actomyosin contractility independently of matrix rigidity [84]. The actin-binding motor protein myosin II maintains a low level of tension on actin fibers that are coupled to the extracellular matrix through cell matrix adhesions. This basal tension enables myosin II to respond to changes in matrix rigidity or elastic behavior by increasing the tension on cell matrix adhesions to activate the GEFs (guanide-exchange factors). These GEFs activate RhoA, which in turn activates ROCK to phosphorylate myosin actin chain (MLC) phosphatase, resulting in an increase of MLC phosphorylation, thereby further increasing myosin II activity and actomyosin-based contractility [85]. This mechanical feedback loop can increase integrin clustering as well as adhesion maturation and might increase intracellular pressure and plasma membrane tension to prevent lamellipodia formation and bleb-based motility. In these experiments, we examined the hypothesis that Rho is activated when cells are in a very stiff substrate, while Rac is activated in environment of low stiffness (0.2 kPa). To test our hypothesis, we used the RhoA pharmacological inhibitor Y-27632, and we examined whether its effect results in Rac1-activation effects on the cells, such as loss of stress fibers and formation of lamellipodia, using immunocytochemistry for α-SMA and fibronectin. We then used the pharmacological inhibitor Z62954982, to test whether Rac1 inhibition forces cells to activate Rho and consequently drives the cells to form stress fibers and become contractile even at environments of low stiffness (0.2 kPa), as it has been shown that RhoA and Rac1 suppress one another's activity [86]. RhoA activity prevents Rac1-stimulated formation of lamellipodia. On the other hand, RhoA-induced contractility is suppressed while Rac1 activity suppresses actomyosin contractility and drives the formation of lamellipodia via enhances actin-mediated protrusions [87]. Here we have shown that myofibroblast differentiation in *Postn*$^{-/-}$ cells was rescued with the addition of Rac inhibitor, suggesting that Periostin modulates myofibroblast differentiation in stiff matrices via RhoA/ROCK pathway.

In this study, we also showed that Postn likely influences the immune response, as shown by the reduced inflammatory cells infiltration in *Postn*$^{-/-}$ wounds. Quantification of macrophage subpopulations during palatal healing shows a significant reduction in both iNOS and arginase-I macrophage populations in *Postn*$^{-/-}$ animals when compared to wild type at day 6 post wounding. During wound healing, macrophages play various roles in

addition to clearing debris by phagocytosis. They secrete enzymes important for collagen production [88] and crosslinking [89], and ECM turn over and resolution [90]. Macrophages also stimulate fibroblast-to-myofibroblast activation [58], an crucial function in tissue repair and fibrosis. On the other hand, myofibroblasts indirectly establish mechanical communication with macrophages by creating stiff ECM as an important environmental cue. Recently, Pakshir & Hinz proposed that contracting (myo)fibroblasts directly transmit mechanical signals through fibrillar ECM that have the potential to attract migratory macrophages [58]. Thus, it is plausible that the reduced recruitment of macrophages in *Postn*$^{-/-}$ is a consequence of reduced myofibroblast differentiation. There is considerable evidence in the literature to support the hypothesis that there is a reduction in macrophage recruitment as a result of periostin deletion. Using a model of arteriosclerosis, it has been shown that wild type macrophages showed enhanced migration in the presence of recombinant periostin protein, an effect not evident in *Postn*$^{-/-}$ macrophages. Moreover, they concluded that *Postn*$^{-/-}$ macrophages show an impaired ability to migrate toward TGF-β [91], which could account for reduced macrophage numbers during wound healing. In addition, it has been demonstrated that periostin itself can act as a chemoattractant for macrophages in a model of glioblastoma [92]. Furthermore, in a renal ischemia-reperfusion injury model, it has been shown that periostin-overexpressing mice exhibit diminished expression of proinflammatory molecules and accumulate more F4/80+ macrophages when compared to periostin knockout mice. Interestingly, both coculturing macrophages with hypoxia-treated primary tubules that overexpress periostin, or alternatively treating macrophages with recombinant periostin, directly induced macrophage proliferation and expression of proregenerative molecules [93]. Periostin has also been strongly implicated in the recruitment of tumor associated macrophages in both intrahepatic cholangiocarcinoma [94] and ovarian cancer [95]. In summary, the reduced number of macrophages in palatal healing likely results from genetic deletion of periostin. Whether this occurs as a result of chemo-attraction or as a result of macrophages expressing periostin is yet to be elucidated in wound healing systems. This will be an area of further investigation for our lab in the future.

Periostin and TGF-β-induced protein (βigh3) are considered paralogs because of their structural similarity, as they both contain a single emilin (EMI) and four fasciclin-1 (FAS1) domains. Similar to periostin, βigh3 is also induced by TGFβ signaling in areas of tissue injury and is secreted by activated fibroblasts [96,97], binds directly to collagens type I, II and IV [98] and localizes to the Golgi apparatus [99]. Here we showed that expression of βigh3 is upregulated during palatal healing, but its expression is reduced in day-6 *Postn*$^{-/-}$ wounds. The alteration in wound closure kinetics in *Postn*$^{-/-}$ animals corresponds with the onset-but not the peak- of Postn expression in WT animals, as well as with the peak of βigh3 expression, indicating that βigh3 may not compensate for the loss of Postn during palatal wound healing. This is further supported by our observations in embryonic tissues where periostin and βigh3 did not exhibit overlapping expression, suggesting that they have independent roles in the development of the hard palate in mice. Recently, Schwanekamp et al. [100] also showed that βigh3 has a distinct function during cardiac healing. After myocardial infarction, deletion of βigh3 does not alter cardiac disease, unlike loss of Postn in Postn$^{-/-}$ mice, and its loss is fully compensated by the more prominently expressed periostin.

In conclusion, in this study we demonstrated that periostin is upregulated during palatal healing in mice, where it is associated with fibronectin production, myofibroblast differentiation and infiltration of macrophages to the wound site. In vitro, *Postn*$^{-/-}$ fibroblasts show reduced contractile ability and fibronectin synthesis, effects which were also modulated by the stiffness of the microenvironment via integrin-β1/RhoA pathway (Fig. 13), providing further evidence that periostin and the stiffness of the ECM act as modulators of matrix synthesis and myofibroblast differentiation during palatal healing. These findings could provide new insights for the development of novel approaches and biomaterials with specific bio-chemical and biomechanical properties targeted to accelerate and enhance the healing process [47], while suppressing fibrosis, after dental and maxillofacial surgical procedures.

Materials and methods

Animals

All animal procedures were in accordance with protocols approved by the University Council on Animal Care at The University of Western Ontario. *Postn*-knockout mice (*Postn*$^{-/-}$) were generated and maintained on soft diet in order to reduce malnutrition, which was previously observed under a standard diet due to the enamel and dentin defects of the incisors and molars [16]. Heterozygous mice were crossed with C57BL/6 J (JAX Mice and Services, Bar Harbor, Maine) for a minimum of six generations to ensure an incipient congenic strain. Backcrossed heterozygous mice were used for breeding and all offspring were genotyped as described previously described [16].

Palatal wounds

For experiments, *Postn*$^{-/-}$ mice (KO) and littermate *Postn*$^{+/+}$ (WT) mice (20weeks of age) were anesthetized with an intraperitoneal injection of buprenorphine (0.05 mg/kg), followed by an injection of ketamine (90 mg/kg) and xylazine (5 mg/kg). One full-thickness excisional wound was made with a 1.5 mm disposable biopsy punch (Integra™ Miltex®, Integra York PA, Inc.) on the hard palate. The localization of the palatal punch biopsy was standardized with the anterior edge of the wound to be aligned with the first molar [101] (Supplemental figure 4) to avoid traumatizing the palatal arteries which run on either side of the wound. The animals received 0.05 mg/kg Buprenorphine by subcutaneous injection twice daily for 48 h post-surgery as an analgesic. Animals were maintained on a standard lab chow powdered food diet and were allowed food and water *ad libitum* for the duration of the experiment. Excised tissue was considered day 0 and was retained as normal healthy tissue. Wounds were photographed immediately after wounding and at time-points selected according to the defined phases of repair: early (day 3), inflammation and granulation tissue formation (day 3, 6), re-epithelialization (completed by day 9) [102], and tissue remodeling (day 12 15). Wound area was assessed from photographs using ImageJ software. Animals were euthanized at 3, 6, 9, 12 and 15 days post-wounding by carbon dioxide inhalation.

Tissue preparation

Post euthanasia, mice were decapitated, and the maxillae were fixed in 10% neutral buffered formalin (Sigma Aldrich,St. Louis, MO) for 24 h and decalcified in 20% EDTA

(ethylenediminetetraacetic acid) for 10 days at 4 °C. The maxillae were dehydrated through a graded series of ethanol, processed and embedded in paraffin, and sectioned at 5 μm thickness for various staining.

Histological analysis

Wounds from WT and *Postn*$^{-/-}$ mice were histologically analysed ($n = 5$) for the extent of re-epithelialization. Sections from the center of the wounds were stained with Masson's Trichrome (University Hospital, London, ON) and wound size as well as epithelial migration distance were calculated using ImageJ software. Epithelial migration distance was defined as the unilateral distance between the wound border and the migrating front of keratinocytes and percentage of epithelialization was determined from bilateral epithelial migration distance, normalized to wound size. Images were taken with a DM1000 light microscope (Leica, Concord, Ontario) and Leica Application Suite Software (version 3.8).

Immunohistochemistry & immunofluorescence

Immunohistochemistry was performed as previously described [25]. Kim et al. *in press*. In brief, tissue sections were deparaffinized, blocked with 10% horse serum, and immune-labeled using primary antibodies against α-smooth muscle actin (α-SMA) (ab5694, 1:200, Abcam plc, Cambridge, United Kingdom) and phosphorylated Smad2/3 (pSmad2/3) (sc11769-R, 1:100, Santa Cruz Biotechnology, Santa Cruz, CA). Sections were counterstained with haematoxylin. Negative controls excluded the primary antibody. Primary antibodies were detected using the ImmPRESS Reagent Kit Peroxidase (Vector Laboratory; Burlingame, CA) and visualized with 3,3-diaminobenzidine DAB reagent (Vector Laboratories) following the manufacturer's instructions. All sections were counterstained with haematoxylin (Sigma Aldrich).

Immunofluorescence staining carried out as above excluding haematoxylin counterstaining. Tissue sections were incubated with primary antibodies against periostin (sc49480, 1:100, Santa Cruz Biotechnology), fibronectin (ab23750, 1:150, Abcam), fibroblast-specific protein-1 was with anti-FSP1/S100A4 (1:100, Millipore, Billerica, MA), Arginase-1 (V:20, sc18354, 1:100, Santa Cruz Biotechnology), iNOS (ab15323, 1:100, Abcam) and Vimentin (ab92547, 1:200, Abcam). Primary antibodies were detected using Alexa Fluor IgG secondary antibodies (Invitrogen, Thermo Fisher Scientific). All sections were counterstained with Hoechst 33,342 dye (1:1000, Invitrogen, Thermo Fisher Scientific) for nuclei. Images were taken on Carl Zeiss Imager M2m microscope (Carl Zeiss, Jena) using ZenPro 2012 software.

RNA isolation and real-time quantitative PCR

Palatal wounded tissues from WT and *Postn*$^{-/-}$ mice ($N = 7$ per timepoint) were dissected using a mm dimeter punch biopsy, homogenized using BeadBug™ prefilled tubes (0.5 mm zirconium beads, Z763772, Sigma-Aldrich) in 1.5 ml of TRIzol reagent (Thermo Fisher Scientific), and purified using RNeasy mini kits (Qiagen, Valencia, CA). The area that was excised for mRNA extraction is shown in Fig. 1C by a white box. Taqman real-time PCR was performed using qSCRIPT XLT one-step real-time quantitative PCR ToughMix (Quanta

Biosciences, Gaithersburg, MD) per the manufacturer's instructions. All samples were run in triplicate and normalized to endogenous 18S rRNA (Thermo Fisher Scientific).

In situ hybridization (ISH)

In situ hybridization for periostin and βigh3 message using antisense and sense (control) *Postn* and *βigh3* cDNA probes (as described Lindsley et al. [103]) was performed on 10 μm paraffin serial sections. For both probes, serial sections were examined using at least three individual palates of each genotype.

Isolation of murine primary palatal fibroblasts (mPFBs)

The soft tissue covering the whole hard palate of six mice was excised and immediately transferred to sterile PBS supplemented with 10% fetal bovine serum and 7x AA (200 U penicillin, 200 mg streptomycin, 0.5 mg/ml amphotericin B) (Gibco, Carlsbad, CA). The tissue was washed 3 times in PBS, 3 times in DMEM, cut into smaller pieces (approx. 1cm^2), and allowed to attach on tissue culture plastic for a few minutes. DMEM, 10% FBS, 1x AA was added and the explants were incubated at 37 °C, 5% CO2 to allow fibroblasts to migrate onto the culture surface. The pieces of palatal tissue were removed, and cells were used at passage 1 and 2 for all experiments.

Cell treatment

mPFBs were seeded in DMEM containing 10% FBS at 8000 cells per cm^2 surface area for RTqPCR and immunocytochemistry, and at 16,000 cells per cm^2 for western blot experiments in 6-well plates of different elastic modulus: 64 kPa, 8 kPa, 0.2 kPa (CytoSoft 6 well plate, Advanced BioMatrix). Tissue culture plastic plates (VWR) served as control. The plates were previously coated with 100 μg/ml collagen type I (PureCol, Advanced BioMatrix, Carlsbad, CA) in DPBS as per manufacturer's instructions. After 24 h, cells were transferred into serum-free DMEM for an additional 16 h. Then 5 ng/mL TGF-β1 (R&D Systems, Minneapolis, MN) was to cells and incubated for 24 to 72 h, depending on the assay. For assessing the influence of FAK pathway inhibition, starved mPPFs were treated with PF-573,228 (10 mM), and DMSO (1:1000) served as a control for PF-573,22. All experiments were run in triplicate.

CyQUANT proliferation assay

After mPFBs from WT and periostin KO animals were seeded on collagen type I pre-coated tissue culture plastic plates as previously described (section 4.9) for 1, 3, 5, and 7 days, media was completely aspirated, and the plates were frozen at −80 °C. Once all time-points were captured, DNA contents were determined by performing CyQUANT® Cell Proliferation Assay Kit (C7026, Molecular Probes). Cell numbers were extrapolated using a standard curve, as per manufacturer's instructions.

Western blotting

mPFBs were cultured on plates of different elastic modulus (8 kPa, 0.2 kPa) coated with 100 μg/ml collagen type I (PureCol, Advanced BioMatrix, Carlsbad, CA) in DPBS for 24 h. Cell lysates were harvested with RIPA buffer (Sigma Aldrich) containing protease

and phosphatase inhibitor cocktails. Protein concentration was determined by Pierce® BCA Protein assay kit (Pierce; Waltham, MA). 12 μg proteins of each sample were separated by sodium dodecyl sulfate polyacrylamide gel electrophoresis (SDS-PAGE) and transferred to nitrocellulose membranes. Membranes were washed with Tris-buffered saline containing 0.05% Tween-20 (TBS-T) and blocked with 5% dried milk in TBS-T or 5% bovine serum albumin (BSA) in TBS-T. Primary antibodies for fibronectin (ab1954, 1:2000, Millipore), α-SMA (A5228, 1:2000, Sigma Aldrich), pFAK Y397 (ab81298, 1:1000, Abcam), FAK (ab40794, 1:1000, Abcam), Vinculin (MAB3574, 1:1000, Millipore), β1-integrin (SAB5600100, 1:1000, Sigma-Aldrich), GAPDH (MAB374, 1:1000, Millipore) were used to incubate the membranes for 12 h. Detection was with appropriate peroxidase-conjugated secondary antibodies (1:2500, Jackson ImmunoResearch; West Grove, PA), which were developed with Clarity Western ECL substrate (Bio-Rad; Hercules, CA). Densitometry analysis was performed using Image Lab Software (Bio-Rad).

Immunocytochemistry

mPFBs were cultured on plates coated with 100 *m*g/ml collagen type I (PureCol, Advanced BioMatrix, Carlsbad, CA) are previously described (section 4.9) for 24 and 72 h. Cells were fixed with 4% paraformaldehyde, permeabilized with 0.1% Triton X-100 and blocked with 1% BSA (Thermo Fisher Scientific). Fixed and permeabilized cells were labeled with mouse anti-α-SMA (A5228, 1:100, Sigma-Aldrich), anti-fibronectin (ab23750, 1:100, Abcam), vinculin (MAB3574, Millipore), β1-integrin (AF2405, R&D Systems) which was detected with appropriate IgG conjugated to Alexa Fluor secondary antibodies (1:100, Invitrogen, Thermo Fisher Scientific). The cells were double immunolabeled with rhodamine-conjugated phalloidin (1:100, Invitrogen) for filamentous actin. Nuclei were counterstained using Hoechst 33,342 dye (1:1000, Thermo Fisher Scientific). Images were taken on Carl Zeiss Imager M2m microscope (Carl Zeiss) using ZenPro 2012 software.

Fixed gel contraction assay

In vitro, contractility of mPFBs was evaluated by employing collagen gel matrix contraction assays as previously described [25,27] mPFBs suspended in 0.5% FBS DMEM were mixed 1:1 with collagen mix [10% 0.2 M HEPES buffer (4-(2-hydroxyethyl)–1 piperazineethanesulfonic acid; pH = 8), 40% bovine collagen type I (Advanced BioMatrix), and 50% 2X high glucose DMEM (Gibco)) to a final density of 100,000 cells/ml. In parallel, either 5 μg/ml rhPN (R&D Systems) or an equivalent volume of PBS was incorporated into the collagen and cell mix. 24 well tissue culture plates were pre-coated with 1% BSA for 12 h and washed with PBS. 1 ml of the cell and collagen mix was plated to each well and allowed to set at 37 °C. Following polymerization, 1 ml of 0.5% FBS DMEM was added to the wells. After 24 h, the gels were detached from the plate and they were left to contract for 24 h at 37 °C. As contraction of the collagen matrix excluded growth medium, thereby reducing the gel weight, loss of gel weight was used to measure the extent of contraction. This accounted for contraction of gels horizontally and vertically.

Statistical analysis

Statistical analysis was by one-way or two-way ANOVA, as appropriate, followed by a Bonferroni correction, using Graphpad Software version 5 (Graphpad Software, La Jolla, CA) ($P<0.05$ was considered significant). For wound healing experiments, data are expressed as a fraction of the original wound area (mean ± SD). *In vivo* gene expression data represents the mean ± standard deviation of seven *Postn*$^{+/+}$ and seven *Postn*$^{-/-}$ wounds for each time point. For quantification of phosphorylated Smad2/3 in the wounds *in vivo*, data are expressed as the percentage of positive cells/total cells per field of view ± standard deviation. For *in vitro* study, data are expressed as the mean ± standard deviation of three individual experiments with independent primary cultures from different animals. Individual experiments included three replicates. For quantification, RT-qPCR, western blot densitometry, gel contraction statistical analysis by two-way ANOVA with Bonferroni multiple comparisons test was used.

Supplementary Material

Refer to Web version on PubMed Central for supplementary material.

Funding

The work is funded by the Canadian Institutes of Health Research Operating Grant to DWH and via National Institutes of Health grant HL135657 to SJC.

Abbreviations:

mPFBS	murine palatal fibroblasts
MPs	matricellular proteins
ECM	extracellular matrix
TR-qPCR	real-time quantitative polymerase chain reaction
ISH	in situ hybridization
TGF-β1	transforming growth factor β1
MMP	matrix metalloproteinase
TIMP	tissue inhibitors of metalloproteinases
SLRPs	small leucine-rich proteoglycans
α-SMA	α-smooth muscle actin
CXCL12	C-X-C motif chemokine 12
OSF-2	osteoblast specific factor 2
BMP-1	Bone morphogenetic protein 1
WT	wild-type

rhPN	human recombinant periostin
FAK	focal adhesion kinase
ROCK	Rho-associated protein kinase
GEFs	guanide-exchange factors
MLC	myosin actin chain
TGFBI/βigh3	transforming growth factor-β-induced gene product-h3

References

[1]. Karamanos NK, Theocharis AD, Neill T, ozzo RVI, Matrix modeling and remodeling: a biological interplay regulating tissue homeostasis and diseases, Matrix Biol 75–76 (2019) 1–11 Jan.

[2]. Smith AJ, Scheven BA, Takahashi Y, Ferracane JL, Shelton RM, Cooper PR, Dentine as a bioactive extracellular matrix, Arch. Oral Biol 57 (2) (2012) 109–121 Feb. [PubMed: 21855856]

[3]. Wong JW, et al. , Wound healing in oral mucosa results in reduced scar formation as compared with skin: evidence from the red Duroc pig model and humans, Wound Repair Regen 17 (5) (2009) 717–729. [PubMed: 19769724]

[4]. Glimet al JE, "Detrimental dermal wound healing: what can we learn from the oral mucosa?"

[5]. Politis C, Schoenaers J, Jacobs R, Agbaje JO, Wound healing problems in the mouth, Front. Physiol 7 (2016) 1–13 no. NOV. [PubMed: 26858649]

[6]. Häkkinen L, Uitto VJ, Larjava H, Cell biology of gingival wound healing, Periodontol 24 (2000) 127–152.

[7]. Dipietro L.a, "Oral mucosal and cutaneous wounds," pp. 621–626, 2003.

[8]. Wijdeveld MGMM, Grupping EM, Kuijpers-Jagtman AM, Maltha JC, Wound healing of the palatal mucoperiosteum in beagle dogs after surgery at different ages, J. Cranio-Maxillo-facial Surg 15 (1987) 51–57.

[9]. Wijdeveld MGMM, Maltha JC, Grupping EM, Dejonge J, Kuijpersjagtman AM, A histological study of tissue-response to simulated cleft-palate surgery at different ages in beagle dogs, Arch. Oral Biol 36 (11) (1991) 837–843. [PubMed: 1763980]

[10]. Larjava H, Wiebe C, Gallant-Behm C, Hart D. a., Heino J, Häkkinen L, Exploring scarless healing of oral soft tissues, J. Can. Dent. Assoc. (Tor) 77 (2011) 1–5 no. C.

[11]. Nanci A, Ten Cate's Oral Histology, vol. 8th ed, Elsevier, 2013, p. 166 Elsevier.

[12]. Walker JT et al., "Cell – matrix interactions governing skin repair : matricellular proteins as diverse modulators of cell function," pp. 73–88, 2015.

[13]. Wells A, Nuschke A, Yates CC, Skin tissue repair: matrix microenvironmental influences, Matrix Biol 49 (2016) 25–36 Jan. [PubMed: 26278492]

[14]. Bornstein P, Sage EH, Matricellular proteins: extracellular modulators of cell function, Curr. Opin. Cell Biol 14 (5) (2002) 608–616. [PubMed: 12231357]

[15]. Hamilton DW, Functional role of periostin in development and wound repair: implications for connective tissue disease, J. Cell Commun. Signal 2 (1–2) (2008) 9–17. [PubMed: 18642132]

[16]. Rios H, et al. , Periostin null mice exhibit dwarfism, incisor enamel defects, and an early-onset periodontal disease-like phenotype, Mol. Cell. Biol 25 (24) (2005) 11131–11144. [PubMed: 16314533]

[17]. Norris RA, et al. , Periostin regulates collagen fibrillogenesis and the biomechanical properties of connective tissues, J. Cell. Biochem 101 (3) (2007) 695–711. [PubMed: 17226767]

[18]. Hwang EY, Jeong MS, Park EK, Kim JH, Jang SB, Structural characterization and interaction of periostin and bone morphogenetic protein for regulation of collagen cross-linking, Biochem. Biophys. Res. Commun 449 (4) (2014) 425–431. [PubMed: 24858685]

[19]. Elliott CG, Hamilton DW, Deconstructing fibrosis research: do pro-fibrotic signals point the way for chronic dermal wound regeneration? J. Cell Commun. Signal 5 (4) (2011) 301–315. [PubMed: 21503732]

[20]. Amizuka N, et al. , Incorporation of Tenascin-C into the extracellular matrix by periostin underlies an extracellular meshwork architecture, J. Biol. Chem 285 (3) (2009) 2028–2039. [PubMed: 19887451]

[21]. Maruhashi T, Kii I, Saito M, Kudo A, Interaction between periostin and BMP-1 promotes proteolytic activation of Lysyl oxidase, J. Biol. Chem 285 (17) (2010) 13294–13303. [PubMed: 20181949]

[22]. Rogers R, et al. , Periostin is required for maturation and extracellular matrix stabilization of noncardiomyocyte lineages of the heart, Circ. Res 102 (7) (2008) 752–760. [PubMed: 18296617]

[23]. Kudo A, Kii I, Periostin function in communication with extracellular matrices, J. Cell Commun. Signal 12 (1) (2018) 301–308. [PubMed: 29086200]

[24]. Zhou H−M, Wang J, Elliott C, Wen W, Hamilton DW, Conway SJ, Spatiotemporal expression of periostin during skin development and incisional wound healing: lessons for human fibrotic scar formation, J. Cell Commun. Signal 4 (2) (2010) 99–107. [PubMed: 20531985]

[25]. Elliott CG, et al. , Periostin modulates myofibroblast differentiation during full-thickness cutaneous wound repair, J. Cell Sci 125 (1) (2012) 121–132. [PubMed: 22266908]

[26]. Crawford J, Nygard K, Gan BS, O'Gorman DB, Periostin induces fibroblast proliferation and myofibroblast persistence in hypertrophic scarring, Exp. Dermatol 24 (2) (2015) 120–126. [PubMed: 25421393]

[27]. Kim SS, Nikoloudaki GE, Michelsons S, Creber K, Hamilton DW, Fibronectin synthesis, but not α-smooth muscle expression, is regulated by periostin in gingival healing through FAK/JNK signaling, Sci. Rep 9 (1) (2019) 2708. [PubMed: 30804350]

[28]. Nikoloudaki G, Creber K, Hamilton DW, Wound healing and fibrosis: a contrasting role for periostin in skin and the oral mucosa, Am. J. Physiol. Physiol (2020).

[29]. Verstappen J, Van Rheden REM, Katsaros C, Torensma R, Von Den Hoff JW, Preferential recruitment of bone marrow-derived cells to rat palatal wounds but not to skin wounds, Arch. Oral Biol 57 (1) (2012) 102–108. [PubMed: 21890107]

[30]. Gabbiani G, Ryan GB, Majne G, Presence of modified fibroblasts in granulation tissue and their possible role in wound contraction, Experientia 27 (5) (May 1971) 549–550. [PubMed: 5132594]

[31]. Tomasek JJ, Gabbiani G, Hinz B, Chaponnier C, Brown R.a, Myofibroblasts and mechano-regulation of connective tissue remodelling, Nat. Rev. Mol. Cell Biol 3 (5) (2002) 349–363. [PubMed: 11988769]

[32]. Hinz B, Myofibroblasts, Exp. Eye Res 142 (2016) 56–70. [PubMed: 26192991]

[33]. Pereira M, Rybarczyk BJ, Odrljin TM, Hocking DC, Sottile J, Simpson-Haidaris PJ, The incorporation of fibrinogen into extracellular matrix is dependent on active assembly of a fibronectin matrix, J. Cell Sci 115 (2002) 609–617 no. Pt 3. [PubMed: 11861767]

[34]. Zollinger AJ, Smith ML, Fibronectin, the extracellular glue, Matrix Biol 60–61 (2017) 27–37.

[35]. Jablonski KA, et al. , Novel markers to delineate murine M1 and M2 macrophages, PLoS ONE 10 (12) (2015) 5–11.

[36]. Kawamoto T, et al. , Structural and phylogenetic analyses of RGD-CAP/beta ig-h3, a fasciclin-like adhesion protein expressed in chick chondrocytes, Biochim. Biophys. Acta 1395 (3) (1998) 288–292. [PubMed: 9512662]

[37]. Bae J−S, et al. , Betaig-h3 supports keratinocyte adhesion, migration, and proliferation through alpha3beta1 integrin, Biochem. Biophys. Res. Commun 294 (5) (2002) 940–948. [PubMed: 12074567]

[38]. LeBaron RG, Bezverkov KI, Zimber MP, Pavelec R, Skonier J, Purchio AF, Beta IG-H3, a novel secretory protein inducible by transforming growth factor-beta, is present in normal skin and promotes the adhesion and spreading of dermal fibroblasts in vitro, J. Invest. Dermatol 104 (5) (1995) 844–849. [PubMed: 7738366]

[39]. Mosher DF, Johansson MW, Gillis ME, Annis DS, Periostin and TGF- β -induced Protein : two Peas in a Pod? Crit. Rev. Biochem. Mol. Biol 50 (5) (2015) 427–439. [PubMed: 26288337]

[40]. Gu L, Zhu YJ, Yang X, Guo ZJ, Xu WB, Tian XL, Effect of TGF-β/Smad signaling pathway on lung myofibroblast differentiation, Acta Pharmacol. Sin 28 (3) (2007) 382–391. [PubMed: 17303001]

[41]. Desmouliére a, Geinoz A, Gabbiani F, Gabbiani G, Transforming growth factor-beta 1 induces alpha-smooth muscle actin expression in granulation tissue myofibroblasts and in quiescent and growing cultured fibroblasts, J. Cell Biol 122 (1) (1993) 103–111. [PubMed: 8314838]

[42]. Humphrey JD, Dufresne ER, Schwartz MA, Mechanotransduction and extracellular matrix homeostasis, Nat. Rev. Mol. Cell Biol 15 (12) (2014) 802–812. [PubMed: 25355505]

[43]. Hinz B, The extracellular matrix and transforming growth factor-β1: tale of a strained relationship, Matrix Biol 47 (2015) 54–65. [PubMed: 25960420]

[44]. Katz BZ, Zamir E, Bershadsky A, Kam Z, Yamada KM, Geiger B, Physical state of the extracellular matrix regulates the structure and molecular composition of cell-matrix adhesions, Mol. Biol. Cell 11 (3) (2000) 1047–1060. [PubMed: 10712519]

[45]. Larjava H, Oral Wound Healing: cell Biology and Clinical Management 2013.

[46]. Lepekhin E, Gron B, Berezin V, Bock E, Dabelsteen E, Differences in motility pattern between human buccal fibroblasts and periodontal and skin fibroblasts, Eur. J. Oral Sci 110 (1) (2002) 13–20. [PubMed: 11878755]

[47]. Urbanczyk M, Layland SL, Schenke-Layland K, The role of extracellular matrix in biomechanics and its impact on bioengineering of cells and 3D tissues, Matrix Biol 85–86 (2020) 1–14.

[48]. Gorin DR, Cordts PR, LaMorte WW, Menzoian JO, The influence of wound geometry on the measurement of wound healing rates in clinical trials, J. Vasc. Surg 23 (3) (1996) 524–528. [PubMed: 8601898]

[49]. D H., Elliott CG, Kim SS, Functional significance of periostin in excisional skin repair. Is the devil in the detail? Cell Adhes. Migr 6 (4) (2012) 319–326.

[50]. Jackson-Boeters L, Wen W, Hamilton DW, Periostin localizes to cells in normal skin, but is associated with the extracellular matrix during wound repair, J. Cell Commun. Signal 3 (2) (2009) 125–133. [PubMed: 19543815]

[51]. Hinz B, Celetta G, Tomasek JJ, Gabbiani G, and Chaponnier C, “Alpha-smooth muscle actin expression upregulates fibroblast contractile activity,” vol. 12, no. September, pp. 2730–2741, 2001.

[52]. Giannopoulou C, Cimasoni G, Functional characteristics of gingival and periodontal ligament fibroblasts, J. Dent. Res 75 (3) (1996) 895–902 Mar. [PubMed: 8675800]

[53]. Gabbiani G, The cellular derivation and the life span of the myofibroblast, Pathol. Res. Pract 192 (7) (1996) 708–711 Jul. [PubMed: 8880871]

[54]. DeLeon-Pennell KY, Barker TH, Lindsey ML, Fibroblasts: the arbiters of extracellular matrix remodeling, Matrix Biol (2020).

[55]. Mah W, et al. , Human gingival fibroblasts display a non-fibrotic phenotype distinct from skin fibroblasts in three-dimensional cultures, PLoS ONE 9 (3) (2014) e90715. [PubMed: 24608113]

[56]. Kim SS, Nikoloudaki G, Darling M, Rieder MJ, Hamilton DW, Phenytoin activates smad3 phosphorylation and periostin expression in drug-induced gingival enlargement, Histol. Histopathol (2019).

[57]. Talele NP, Fradette J, Davies JE, Kapus A, Hinz B, Expression of α-smooth muscle actin determines the fate of mesenchymal stromal cells, Stem. Cell Rep 4 (6) (2015) 1016–1030.

[58]. Pakshir P, Hinz B, The big five in fibrosis: macrophages, myofibroblasts, matrix, mechanics, and miscommunication, Matrix Biol 68–69 (2018) 81–93.

[59]. Walraven M, Hinz B, Therapeutic approaches to control tissue repair and fibrosis: extracellular matrix as a game changer, Matrix Biol 71–72 (2018) 205–224.

[60]. Leask A, Focal Adhesion Kinase: a Key Mediator of Transforming Growth Factor Beta Signaling in Fibroblasts, Advances in Wound Care, 2013.

[61]. Goffin JM, Pittet P, Csucs G, Lussi JW, Meister JJ, Hinz B, Focal adhesion size controls tension-dependent recruitment of α-smooth muscle actin to stress fibers, J. Cell Biol 172 (2) (2006) 259–268. [PubMed: 16401722]

[62]. Achterberg VF, et al. , The nano-scale mechanical properties of the extracellular matrix regulate dermal fibroblast function, J. Invest. Dermatol 134 (7) (2014) 1862–1872. [PubMed: 24670384]

[63]. Rousselle P, Montmasson M, Garnier C, Extracellular matrix contribution to skin wound re-epithelialization, Matrix Biol 75–76 (2019) 12–26 Jan.

[64]. Hinz B, The myofibroblast: paradigm for a mechanically active cell, J. Biomech 43 (1) (2010) 146–155. [PubMed: 19800625]

[65]. Winer JP, Janmey PA, McCormick ME, Funaki M, Bone Marrow-Derived Human Mesenchymal Stem Cells Become Quiescent on Soft Substrates but Remain Responsive to Chemical or Mechanical Stimuli, Tissue Eng. Part A, 2008.

[66]. Olsen M, Abby LUemura, et al. , Hepatic stellate cells require a stiff environment for myofibroblastic differentiation, Am. J. Physiol. Liver Physiol 301 (1) (2011) G110–G118.

[67]. Serini G, et al. , The Fibronectin Domain ED-A Is Crucial for Myofibroblastic Phenotype Induction by Transforming Growth Factor-β1, J. Cell Biol 142 (3) (2002) 873–881.

[68]. Klingberg F, et al. , The fibronectin ED-A domain enhances recruitment of latent TGF-β-binding protein-1 to the fibroblast matrix, J. Cell Sci 131 (5) (2018) p. jcs201293. [PubMed: 29361522]

[69]. Singh P, Carraher C, Schwarzbauer JE, Assembly of Fibronectin Extracellular Matrix, Annu. Rev. Cell Dev. Biol (2010).

[70]. Mao Y, Schwarzbauer JE, Fibronectin fibrillogenesis, a cell-mediated matrix assembly process, Matrix Biol (2005).

[71]. Koli K, Hyytiäinen M, Ryynänen MJ, Keski-Oja J, Sequential deposition of latent TGF-β binding proteins (LTBPs) during formation of the extracellular matrix in human lung fibroblasts, Exp. Cell Res 310 (2) (2005) 370–382 Nov. [PubMed: 16157329]

[72]. Kii I, et al. , Incorporation of Tenascin-C into the extracellular matrix by periostin underlies an extracellular meshwork architecture, J. Biol. Chem 285 (3) (2009) 2028–2039. [PubMed: 19887451]

[73]. Kii I, Nishiyama T, Kudo A, Periostin promotes secretion of fibronectin from the endoplasmic reticulum, Biochem. Biophys. Res. Commun 470 (4) (2016) 888–893. [PubMed: 26820539]

[74]. Moore SW, Roca-Cusachs P, Sheetz MP, Stretchy proteins on stretchy substrates: the important elements of integrin-mediated rigidity sensing, Dev. Cell 19 (2) (2010) 194–206. [PubMed: 20708583]

[75]. Schwarz US, Gardel ML, United we stand – integrating the actin cytoskeleton and cell – matrix adhesions in cellular mechanotransduction, J. Cell Sci 125 (13) (2012) 3051–3060. [PubMed: 22797913]

[76]. Danen EHJ, Sonneveld P, Brakebusch C, Fässler R, Sonnenberg A, The fibronectin-binding integrins α5β1 and αvβ3 differentially modulate RhoA-GTP loading, organization of cell matrix adhesions, and fibronectin fibrillogenesis, J. Cell Biol 159 (6) (2002) 1071–1086. [PubMed: 12486108]

[77]. Guilluy C, Swaminathan V, Garcia-Mata R, O'Brien ET, Superfine R, Burridge K, The Rho GEFs LARG and GEF-H1 regulate the mechanical response to force on integrins, Nat. Cell Biol (2011).

[78]. Engler AJ, Sen S, Sweeney HL, Discher DE, Matrix elasticity directs stem cell lineage specification, Cell 126 (4) (2006) 677–689. [PubMed: 16923388]

[79]. Pelham RJ, Wang YL, Cell locomotion and focal adhesions are regulated by the mechanical properties of the substrate, Biol. Bull 194 (3) (1998) 348–350. [PubMed: 11536880]

[80]. Maekawa M, et al. , Signaling from Rho to the actin cytoskeleton through protein kinases ROCK and LIM-kinase, Science (80-.) 285 (5429) (1999) 895–898 Aug.

[81]. van der Bijl I, et al. , Reciprocal integrin/integrin antagonism through kindlin-2 and Rho GTPases regulates cell cohesion and collective migration, Matrix Biol (2020) May.

[82]. Yoneda A, Multhaupt HAB, Couchman JR, The Rho kinases I and II regulate different aspects of myosin II activity, J. Cell Biol (2005).

[83]. Yoneda A, Ushakov D, Multhaupt HAB, Couchman JR, Fibronectin matrix assembly requires distinct contributions from Rho Kinases I and -II, Mol. Biol. Cell (2006).

[84]. Ridley AJ, Hall A, The small GTP-binding protein rho regulates the assembly of focal adhesions and actin stress fibers in response to growth factors, Cell 70 (3) (1992) 389–399. [PubMed: 1643657]

[85]. Nakano K, et al. , Distinct actions and cooperative roles of ROCK and mDia in Rho Small G Protein-induced Reorganization of the Actin Cytoskeleton in Madin-Darby Canine Kidney Cells, Mol. Biol. Cell 10 (8) (2013) 2481–2491.

[86]. Higashida C, et al. , ROCK and mDia1 antagonize in Rho-dependent Rac activation in Swiss 3T3 fibroblasts, J. Cell Biol (2002).

[87]. Huveneers S, Danen EHJ, Adhesion signaling - crosstalk between integrins, Src and Rho, J. Cell Sci 122 (8) (2009) 1059–1069. [PubMed: 19339545]

[88]. Hesse M, et al. , Differential Regulation of Nitric Oxide Synthase-2 and Arginase-1 by Type 1/Type 2 Cytokines In Vivo: granulomatous Pathology Is Shaped by the Pattern of L-Arginine Metabolism, J. Immunol 167 (11) (2014) 6533–6544.

[89]. Lupher ML, Gallatin WM, Regulation of Fibrosis by the Immune System, Adv. Immunol (2006).

[90]. Sprangers S, Everts V, Molecular pathways of cell-mediated degradation of fibrillar collagen, Matrix Biol (2017).

[91]. Schwanekamp JA, Lorts A, Vagnozzi RJ, Vanhoutte D, Molkentin JD, Deletion of periostin protects against atherosclerosis in mice by altering inflammation and extracellular matrix remodeling, Arterioscler. Thromb. Vasc. Biol 36 (1) (Jan. 2016) 60–68. [PubMed: 26564821]

[92]. Squadrito ML, De Palma M, A niche role for periostin and macrophages in glioblastoma, Nat. Cell Biol 17 (2) (2015) 107–109. [PubMed: 25633271]

[93]. Kormann R, et al. , Periostin promotes cell proliferation and macrophage polarization to drive repair after AKI, J. Am. Soc. Nephrol 31 (1) (2020) 85–100 Jan. [PubMed: 31690575]

[94]. Zeng J, et al. , Tumor-associated macrophages recruited by periostin in intrahepatic cholangiocarcinoma stem cells, Oncol. Lett 15 (6) (2018) 8681–8686 Jun. [PubMed: 29805605]

[95]. Tang M, Liu B, Bu X, Zhao P, Cross-talk between ovarian cancer cells and macrophages through periostin promotes macrophage recruitment, Cancer Sci 109 (5) (2018) 1309–1318 May. [PubMed: 29527764]

[96]. Skonier J, Neubauer M, Madisen L, Bennett K, Plowman G, Purchio A, cDNA cloning and sequence analysis of beta ig-h3, a novel gene induced in a human adeno-carcinoma cell line after treatment with transforming growth factor-beta, DNA Cell Biol (1992).

[97]. Holmberg C, et al. , Release of TGFβig-h3 by gastric myofibroblasts slows tumor growth and is decreased with cancer progression, Carcinogenesis (2012).

[98]. Hashimoto K, et al. , Characterization of a cartilage-derived 66-kDa protein (RCD-CAP/big-h3) that binds to collagen, Biochim. Biophys. Acta - Mol. Cell Res (1997).

[99]. Kim BY, et al. , Corneal dystrophy-associated R124H mutation disrupts TGFBI interaction with periostin and causes mislocalization to the lysosome, J. Biol. Chem (2009).

[100]. Schwanekamp JA, et al. , TGFBI functions similar to periostin but is uniquely dispensable during cardiac injury, PLoS ONE 12 (7) (2017).

[101]. Keswani SG, et al. , Role of salivary vascular endothelial growth factor (VEGF) in palatal mucosal wound healing, Wound Repair Regen 21 (4) (2013) 554–562. [PubMed: 23758212]

[102]. Cornelissen a M., Maltha JC, Von den Hoff HW, Kuijpers-Jagtman a M., Palatal mucoperiosteal wound healing in the rat, Eur. J. Oral Sci 107 (5) (1999) 344–351. [PubMed: 10515199]

[103]. Lindsley A, Li W, Wang J, Maeda N, Rogers R, Conway SJ, Comparison of the four mouse fasciclin-containing genes expression patterns during valvuloseptal morphogenesis, Gene Expr. Patterns (2005).

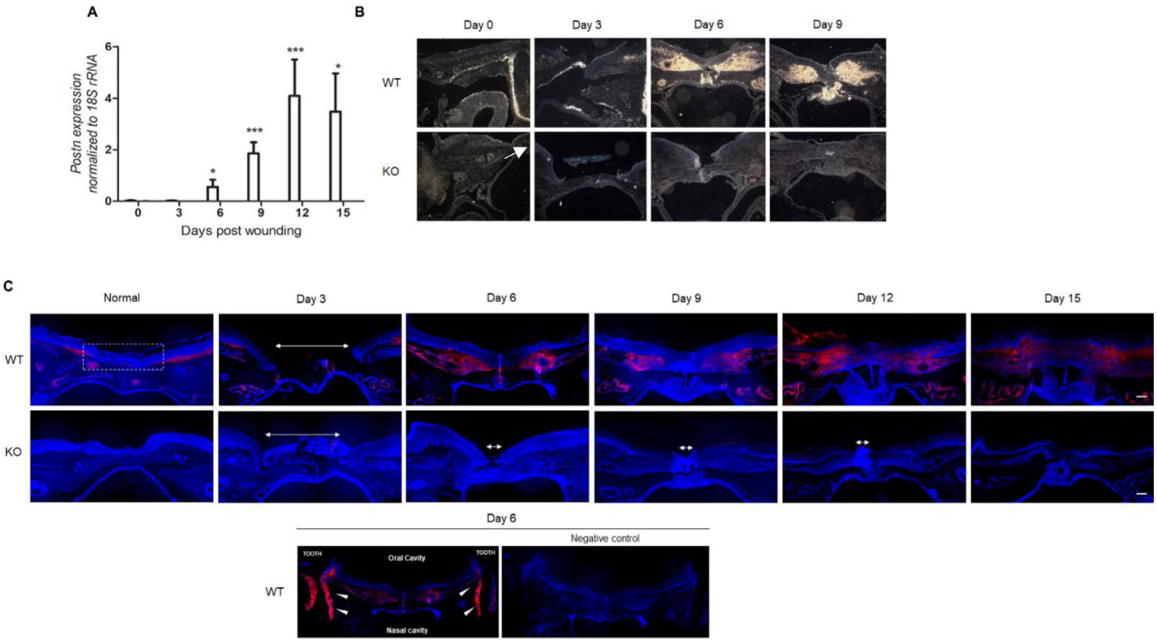

Fig. 1.

Periostin mRNA and protein are up-regulated after excisional palatal wounding

1.5 mm full-thickness excisional wounds were created on the hard palate of periostin-knockout (Postn$^{-/-}$) and wild-type (WT) mice. (A) Postn mRNA expression was quantified in tissues from 0 to 15 days post wounding using quantitative PCR. Values are given as mean ± SD. Data was analyzed using one-way ANOVA $N = 7$ for each time-point (*$P < 0.05$; ***$P < 0.001$ comparisons to d0). All samples were run in triplicate and normalized to endogenous 18S rRNA (B) Periostin mRNA message detection in d0, d3, d6, d9 wounds of WT and Postn$^{-/-}$ mice by In Situ Hybridization (C) Immunofluorescent staining for Periostin from d0 to d15 post-wounding. White box indicates the area that was excised for mRNA extraction. White arrows indicate the length of the open wounds. White arrowheads indicate the periodontal ligament of the teeth. Scale bar: 200 μm.

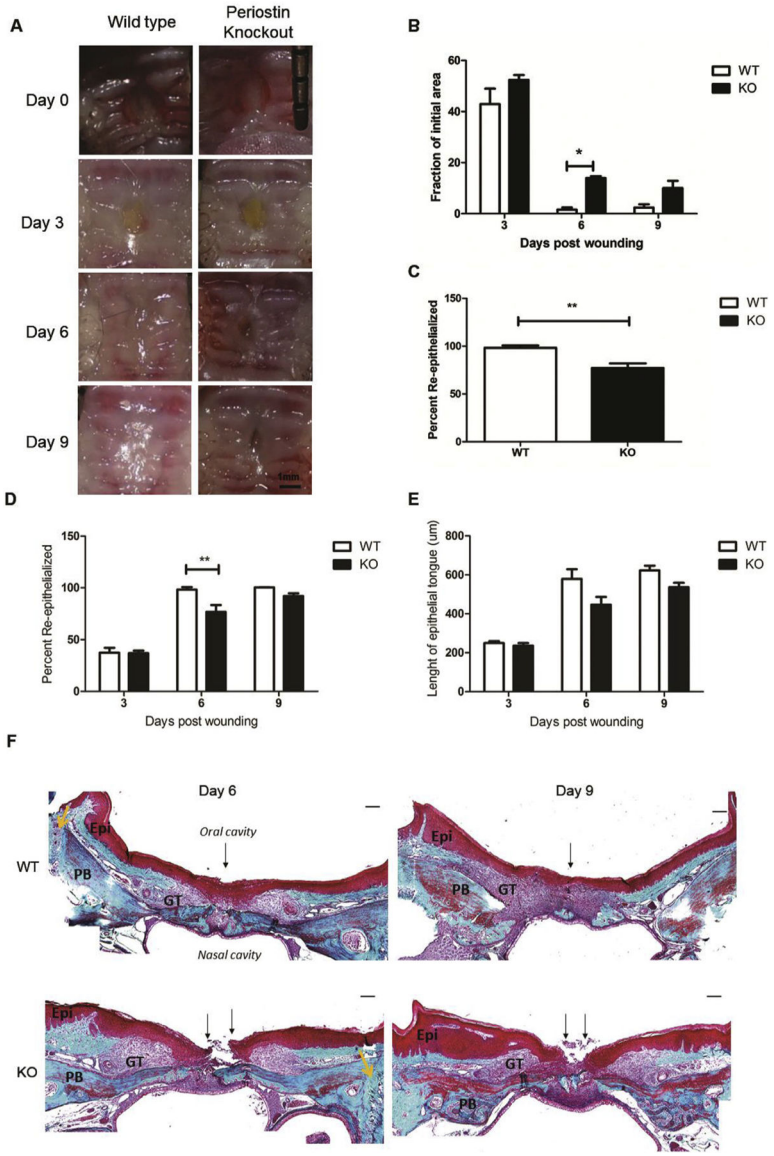

Fig. 2. Genetic deletion of periostin results in altered wound-closure kinetics during excisional palatal healing in mice

(A) Wound size was measured up to 12 days post wounding in 1.5-mm wounds from 7 *Postn*$^{-/-}$ and 7 WT animals. Representative wounds are shown at 0, 3, 6, and 9 days post wounding (top to bottom). Bar= 1 mm. Masson's tri-chrome-stained sections were used to analyze wound size (B), re-epithelialization (C, D) and the epithelial tongue length (E). 5 *Postn*$^{-/-}$ and 5 WT mice were quantified. Data are expressed as mean ± standard deviation. $*P < 0.05$; $**P < 0.01$. (F) **Representative images from sections stained with Masson's Trichrome Stain**. WT wounds have completely closed by day 6. However, *Postn*$^{-/-}$ wounds present delayed healing as at day 9 reepithelialization has not been completed. Black arrows indicate edge of the wound. Yellow arrows indicate the periodontal ligament of neighbouring teeth. (**PB**= Palatal Bone, **Epi**= oral Epithelium, **GT**= Granulation Tissue) Scale bar= 125 μm

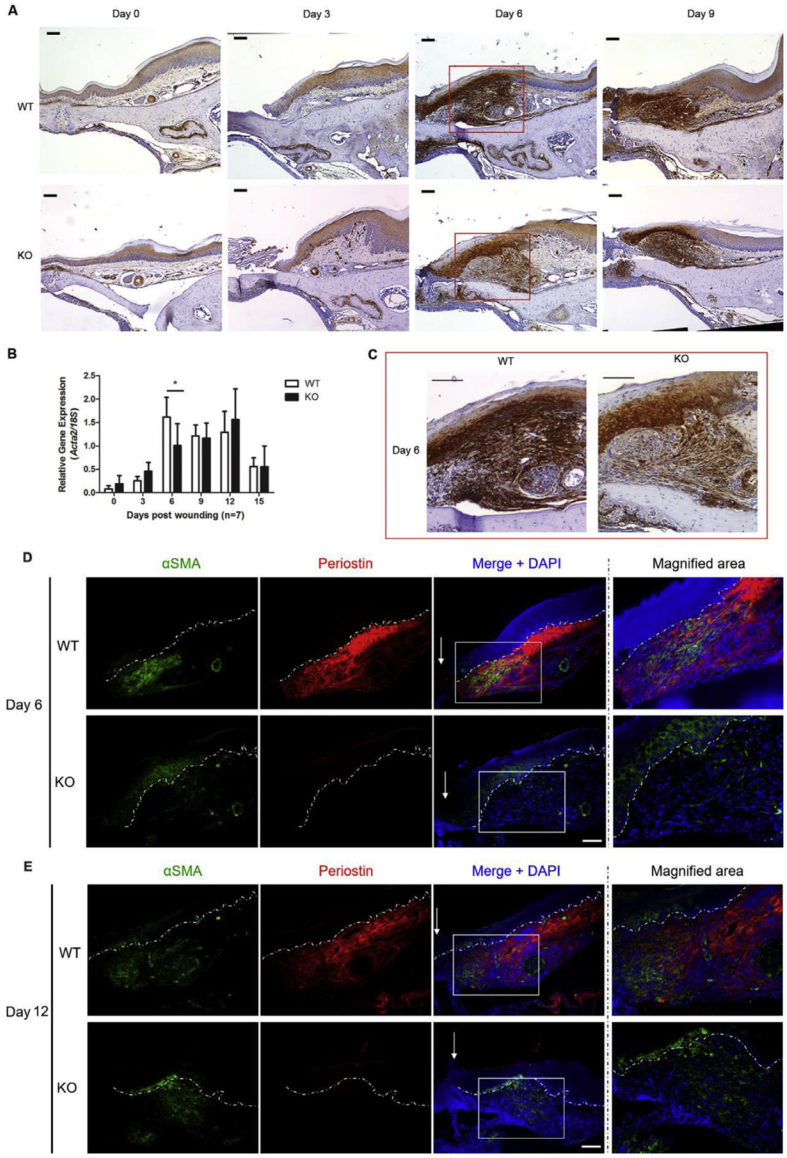

Fig. 3. α-SMA expression is reduced, but not absent, in the granulation tissue of *Postn*$^{-/-}$ mice

(A) Immunohistochemical staining for α-smooth muscle actin (α-SMA). Sections of normal (day 0) tissue and day 3,6 and 9 wounds of WT and *Postn*$^{-/-}$ animals. The area highlighted in the red rectangle is magnified below in panel **(C)**. **(B)** *Acta2* expression was quantified in tissue from 3 to 15 days post wounding using RTqPCR. Values are given as mean±SD. $N = 7$ animals per time point. $*P < 0.05$. **(D)** Double immunofluorescent staining to detect α-SMA (green) and periostin (red) signal at day 6 and day 12 wounds of WT and *Postn*$^{-/-}$ animals. Scale bar: 100 μm. White dashed lines indicate the border between the epithelium and the granulation tissue.

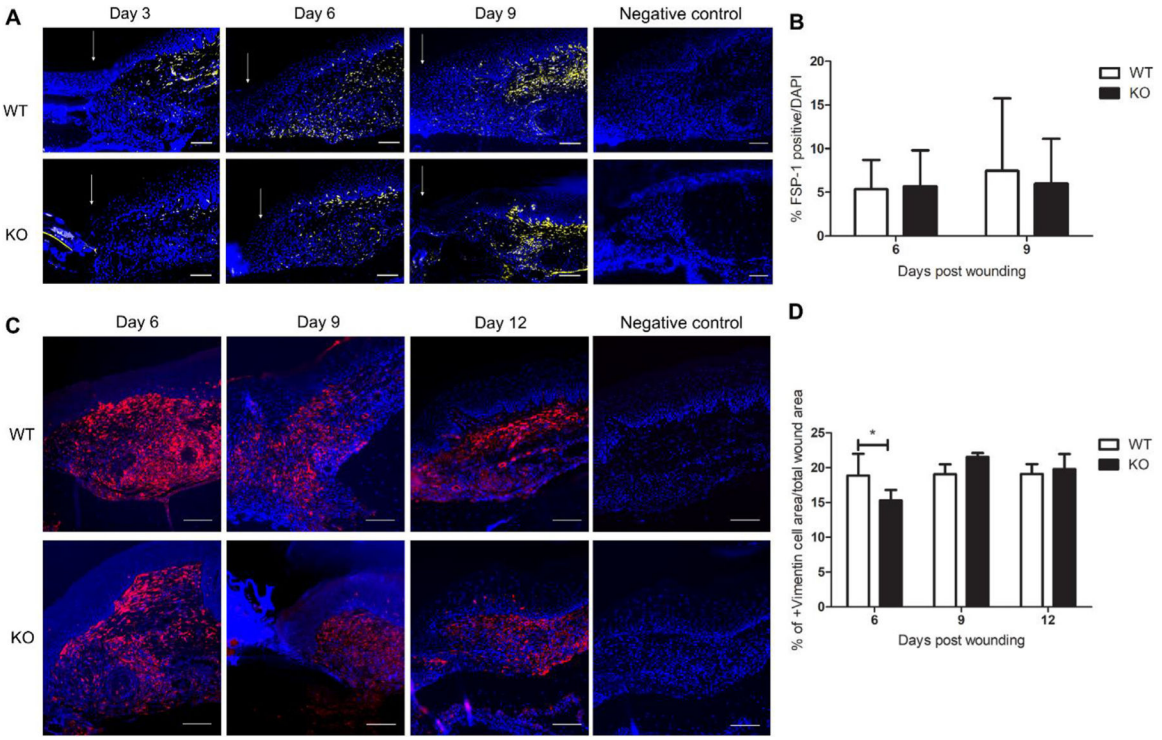

Fig. 4.

(A) Immunofluorescent staining to detect fibroblasts using fibroblast-specific protein-1 antibody. Bar: 200 μm. ***(B)*** Quantification presented as percentage of FSP-1-positive cells/DAPI-positive cells of wounds at days 6 and 9 post-wounding, in four WT and four Postn$^{-/-}$ mice. ***(C)*** Immunofluorescent staining for Vimentin. ***(D)*** Quantification presented as percentage of Vimentin positive area/wound area of wounds at days 6, 9 and 12 post-wounding, in four WT and four Postn$^{-/-}$ mice. Bar: 200 μm. ($P < 0.05$) White arrows indicate the leading wound edge.

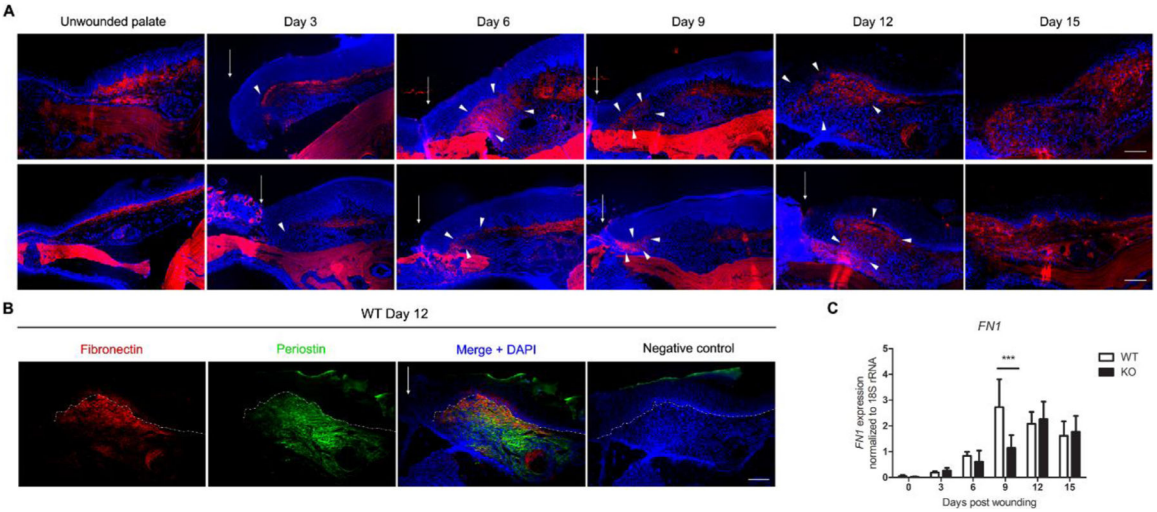

Fig. 5. Genetic deletion of Postn is associated with reduced fibronectin expression and deposition during palatal healing

(A) Representative images of immunoreactivity for Fibronectin of unwounded (day 0) and wounded mice palate. White arrows indicate the leading wound edge and white arrowheads indicate fibronectin labeling in the granulation tissue at the wound edge. Scale bar: 200 μm. **(B)** Double immunofluorescent staining to detect periostin (green) and fibronectin (red) localization in the granulation tissue day 12 wounds of WT animals. Scale bar: 100 μm **(C)** FN1 mRNA expression was quantified in tissues from 0 to 15 days post wounding using quantitative PCR. Values are given as mean±SD. Data was analyzed using one-way ANOVA $N = 7$ for each time-point (***$P < 0.001$).

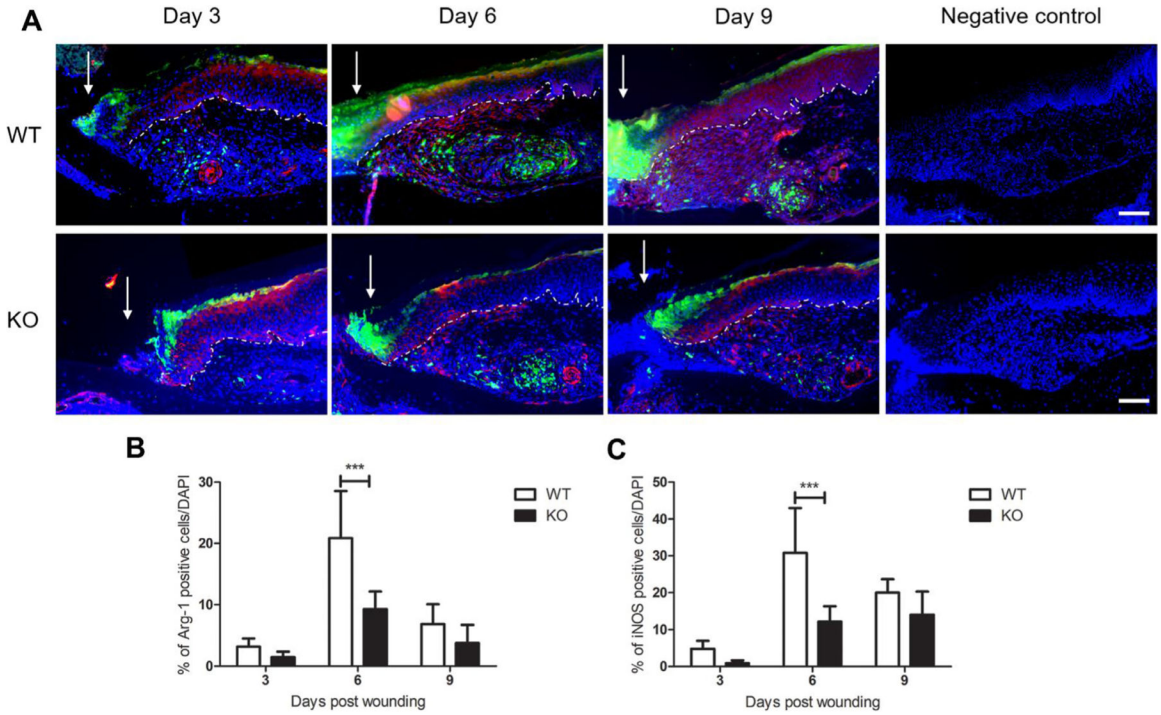

Fig. 6. Genetic deletion of Postn affects immune cell infiltration.

(A) Double Immunofluorescent staining to detect macrophages markers **Arginase-1** (M2 polarization-green) (Arg-1, V:20 sc18354) and **iNOS** (M1 polarization-red) (iNOS antibody ab15323). White arrows indicate the leading edge of the wound. White dashed line indicates the border between the epithelium and the granulation tissue. Scale bar: 200 μm. **(B)** Quantification presented as percentage of Arginase-1-positive cells/DAPI positive cells of wounds at days 3, 6 and 9 post-wounding, in six WT and four Postn$^{-/-}$ mice. **(C)** Quantification presented as percentage of iNOS-positive cells/DAPI positive cells of wounds at days 3, 6 and 9 post-wounding, in six WT and four Postn$^{-/-}$ mice.

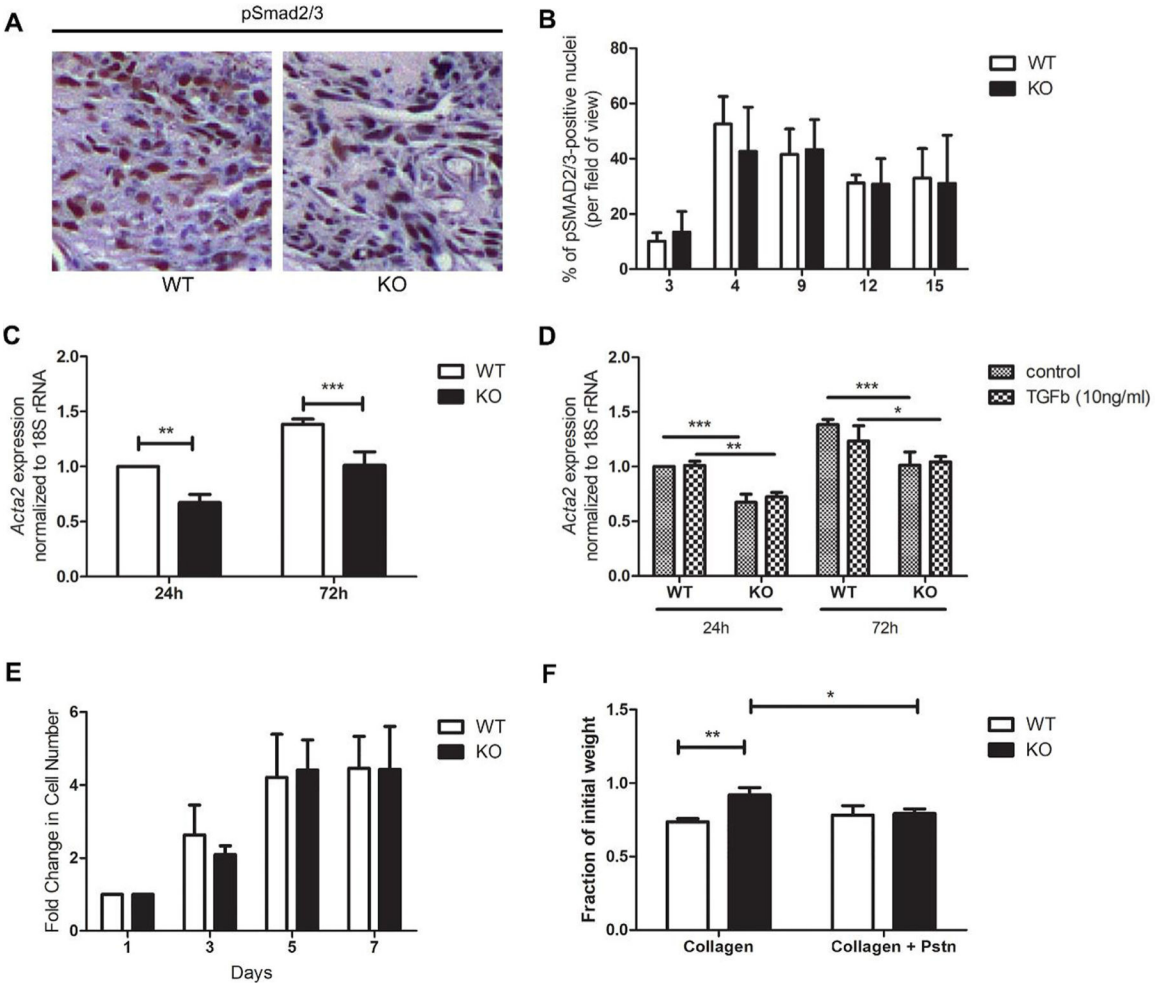

Fig. 7. Canonical TGFβ signaling is not altered in Postn$^{-/-}$ fibroblasts & Exogenous periostin is sufficient to induce a contractile phenotype

(A) Immunohistochemical staining for phosphorylated Smad2/3 (Santa Cruz sc11769). Detection was with peroxidase-conjugated secondary antibodies-chromogen DAB. Representative images of wounds at day 6 post-wounding in WT and Postn$^{-/-}$ animals. **(B)** Numbers of positively stained nuclei per field of view were not significantly different between WT and Postn$^{-/-}$ (KO) wounds. **(C, D)** WT and *Postn-/*mPFBs were seeded on TCP, with or without TGFβ (5 ng/ml). At 24- and 72-hours Acta2 expression was quantified using RTqPCR. Data represents mean fold gene expressions ±SD relative to control 24 h (without TGFβ-control) of 3 independent experiments in triplicates ($N = 3$, $n = 3$ per time point. *$P < 0.05$, **$P<0.01$, ***$P<0.001$, two-way AVONA) **(E)** WT and KO mPFBs cultured for 1, 3, 5, and 7 days were assessed for proliferation using CyQUANT assay kit to determine DNA contents. A standard curve was used to extrapolate cell number. Data represents fold cell number increase ±SD relative to day 1. Data was analyzed via two-way ANOVA ($p > 0.05$). **(F)** Gel contraction was quantified by loss of gel weight, compared with gels lacking cells. *Postn*$^{-/-}$ (KO) fibroblasts were unable to significantly contract collagen gels. WT fibroblasts were able to contract collagen gels. Exogenous addition of 5 mg/ml rhPstn to the collagen gels rescued the contractile ability of *Postn*$^{-/-}$ fibroblasts. Data is

expressed as a fraction of the initial gel weight; error bars represent SD ($N = 3$, $n = 3$, $*P < 0.05$, $**P < 0.01$, two-way ANOVA).

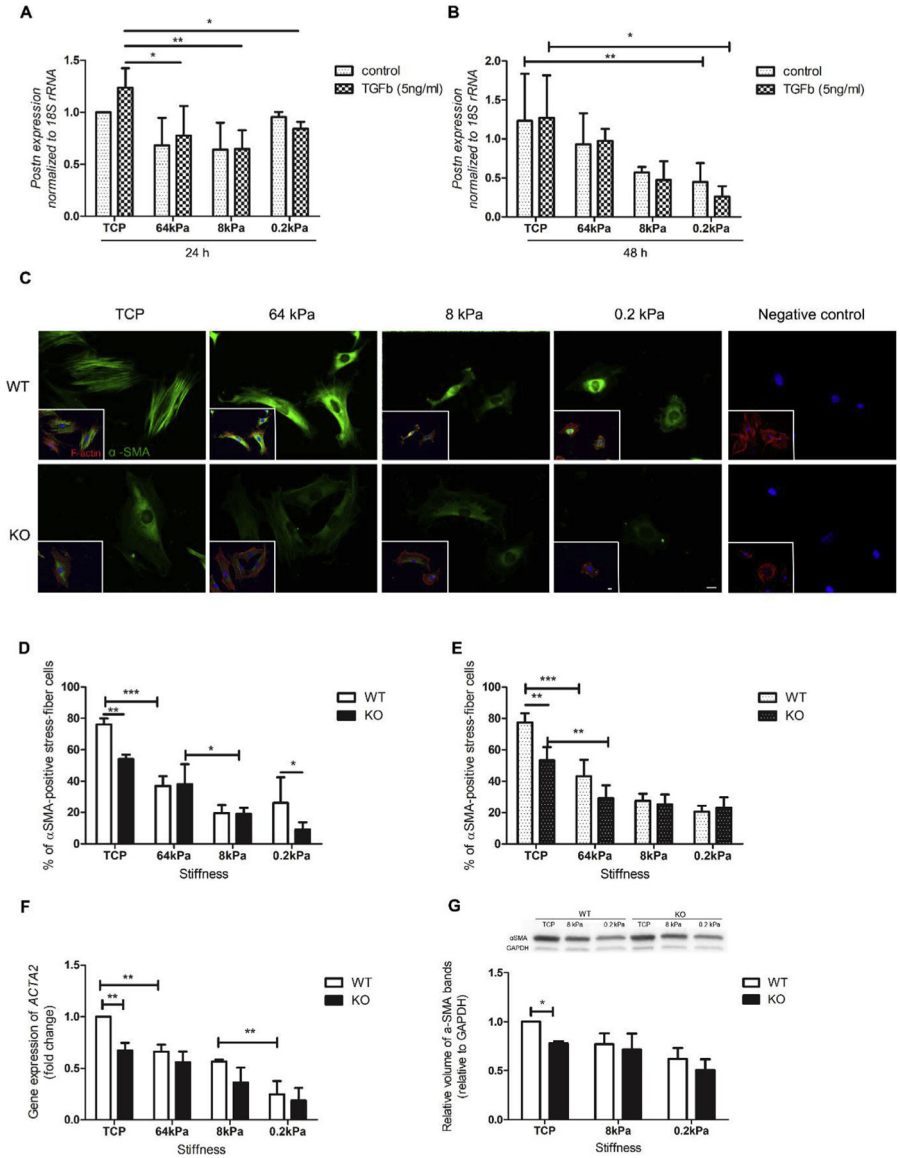

Fig. 8.

(A, B) Periostin expression in mPFBs is regulated by matrix stiffness: WT mPFBs were cultured on silicone substrates of different stiffness, with or without TGFβ, for (A) 24- and (B) 72-hours, and *Postn* mRNA levels were quantified using RTqPCR. Values are given as mean±SD from 3 independent experiments. Data was analyzed using ANOVA, (*$P < 0.05$; **$P < 0.005$). **(C)** Matrix stiffness alone is not sufficient to restore the contractile phenotype of *Postn*$^{-/-}$ cells: mPFBs were cultured on silicone substrates of different stiffness and analysed for α-SMA incorporation in stress fibers. **(D)** Quantification of α-SMA positive stress fiber-cells. **(E)** mPFBs were treated with 5 ng/ml TGFβ and α-SMA positive stress fiber-cells were quantified using immunofluorescence. **(F)** *Acta2* expression was quantified RTqPCR. (G) Western blot was used to assess α-SMA protein level of WT and *Postn*$^{-/-}$ mPFBs. GAPDH was used as a loading control. Values are given as mean±SD from 3

independent experiments. Data was analyzed using ANOVA, (*$P < 0.05$; **$P < 0.005$). Scale bar: 20 μm.

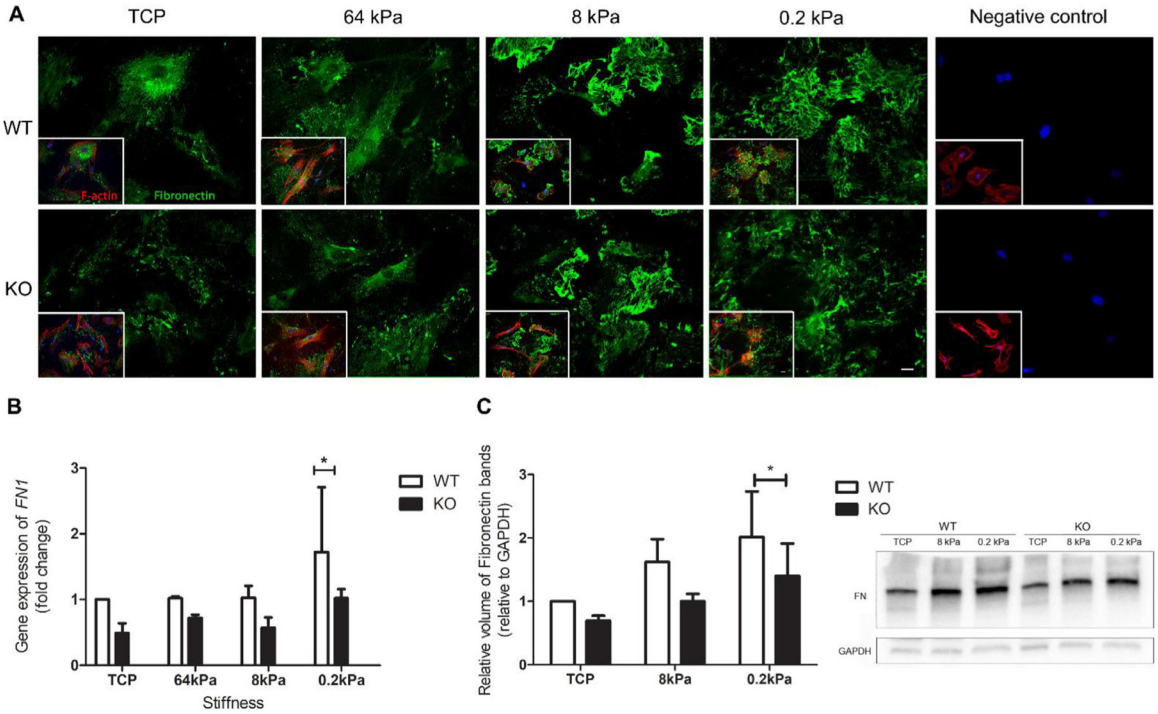

Fig. 9. Fibronectin secretion is regulated by Periostin and Matrix stiffness.

(A) mPFBs were cultured on silicone substrates of different stiffness and analysed for Fibronectin secretion using immunofluorescence. **(B)** *FN1* expression was quantified using RTqPCT. (C) Western blot was used to assess fibronectin protein level of WT and Postn$^{-/-}$ mPFBs. GAPDH was used as a loading control. Values are given as mean±SD from 3 independent experiments. Data was analyzed using ANOVA, (*$P < 0.05$). Scale bar: 20 μm.

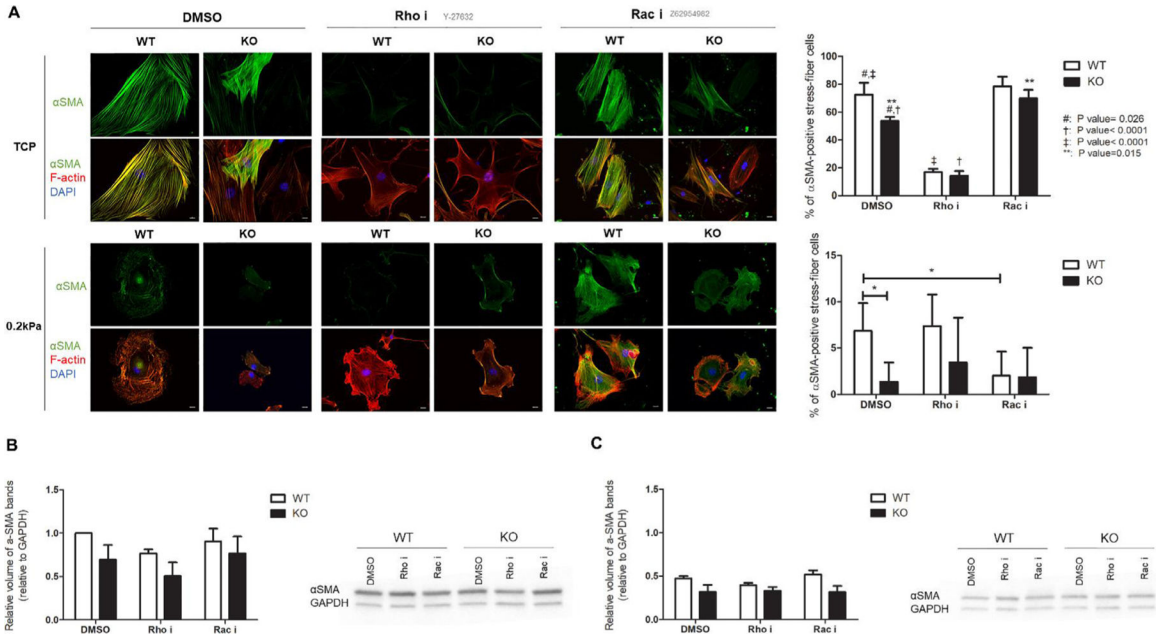

Fig. 10. Periostin modulates myofibroblast differentiation in mPFBs via RhoA pathway.

(A) mPFBs were cultured on TCP (top row) or silicon substrates with 0.2 kPa Young's modulus of elasticity (bottom row), treated with pharmacological inhibitors for RhoA, Y-27632 (10 μM), and Rac1, Z62954982 (50 μM), and analysed for α-SMA incorporation in stress fibers using immunofluorescence and Western Blotting. Western blot was used to assess α-SMA protein level of WT and *Postn*$^{-/-}$ mPFBs on TCP (B) and 0.2 kPa substrate (C). GAPDH was used as a loading control. Values are given as mean±SD from 3 independent experiments. Data was analyzed using ANOVA, (*$P < 0.05$; **$P < 0.005$). Scale bar: 20 μm.

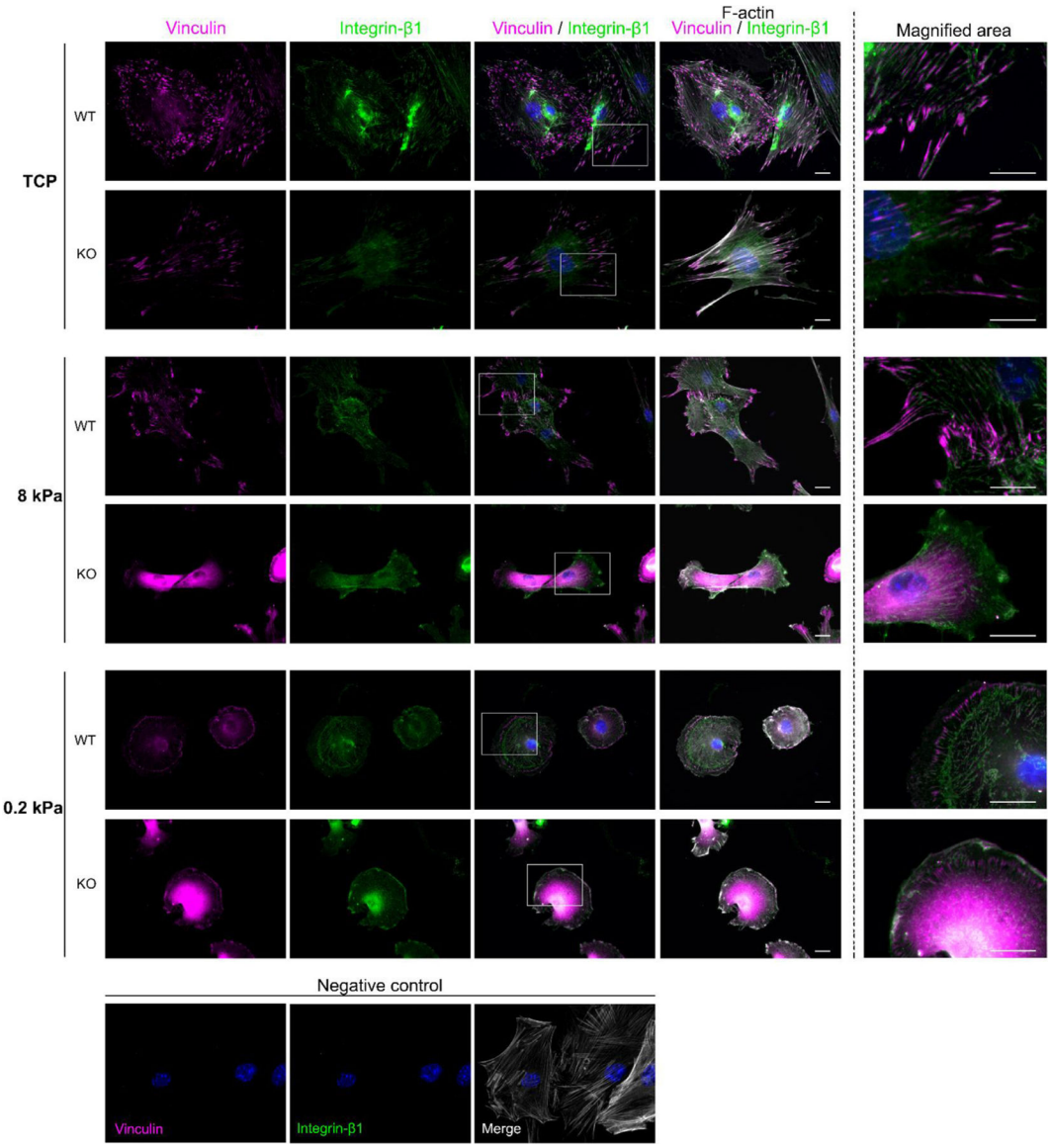

Fig. 11. Periostin is required for the formation of focal and fibrillar adhesions in mPFBs.

mPFBs were cultured on silicone substrates of different stiffness and analysed for focal (Vinculin) and fibrillar (integrin-β1) adhesions formation using immunocytochemistry. Representative images of immunoreactivity for Vinculin (magenta) and integrin-β1 (green). Nuclei are stained with Hoechst 33,342 dye (blue) F-actin with white. Scale bar: 20 μm.

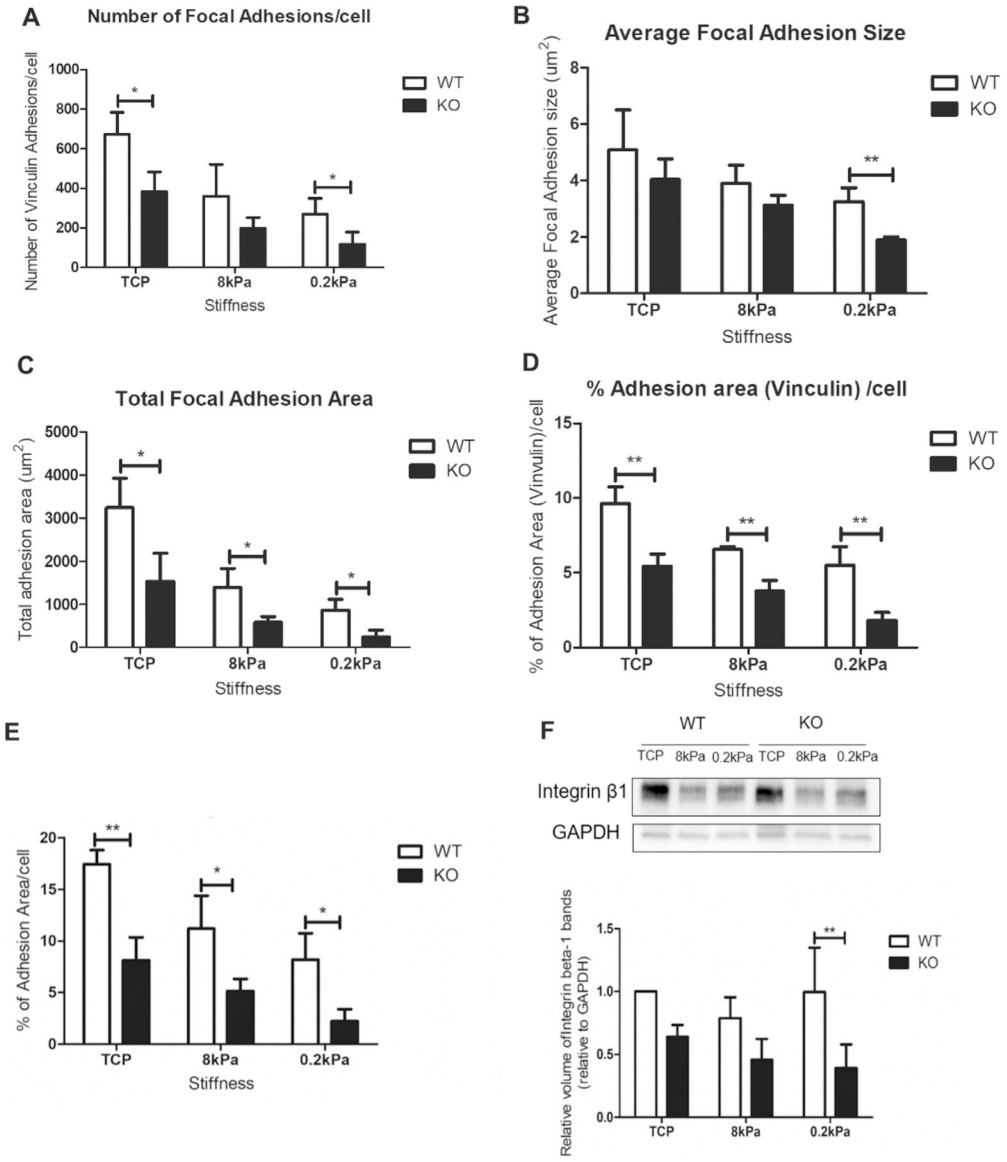

Fig. 12. Periostin is required for the formation of focal and fibrillar adhesions in mPFBs

Immunostaining for focal (Vinculin-positive) adhesions was used to quantify: **(A)** the number of focal adhesions/cell, **(B)** the average focal adhesion size, **(C)** the total adhesion area (μm^2), and **(D)** the% of focal adhesion area/cell. **(E)** Fibrillar adhesion formation expressed as% of adhesion area/cells was quantified using immunostaining for integrin-β1, **(F)** Integrin-β1 levels were quantified using Western Blotting. Values are given as mean±SD from 3 independent experiments. Data was analyzed using ANOVA. (*P<0.05, **P<0.005).

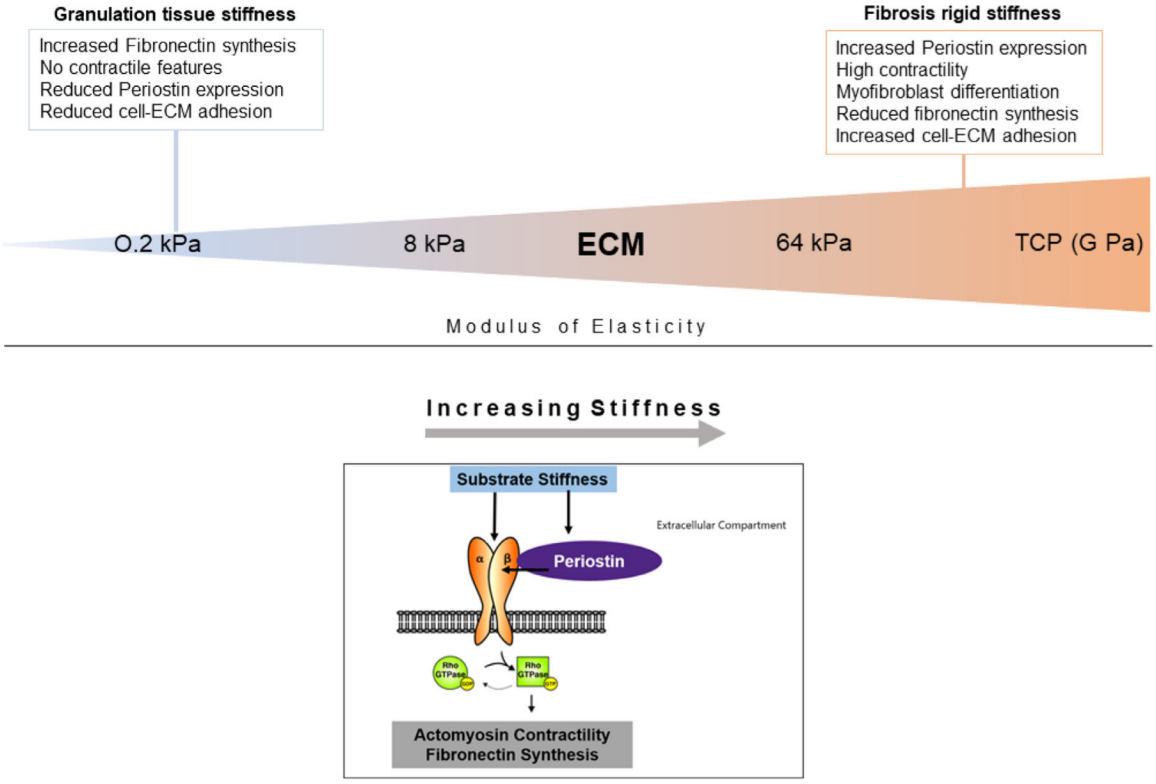

Fig. 13. Proposed Mechanism.

The biomechanical propertied of a tissue in terms of stiffness (modulus of elasticity) vary across the different phases of wound healing. During the early phases of wound healing, the loose newly formed granulation tissue exhibits low stiffness, while, as the healing process progresses, the stiffness of the tissue increases with the deposit and remodeling of the ECM. Here, we demonstrate how the cellular behavior is modulated by the matrix stiffness, the molecular events that govern this process, as well as the role of periostin in palatal wound healing.